A Radar Power Multiplier Algorithm for Acquisition of Low Observable Ballistic Missiles Using an ESA Radar*

Sivaloganathan Sivananthan†
Air Traffic Control Division
ARCON Corporation
Waltham MA 02451-1080, USA.

Thiagalingam Kirubarajan‡ and Yaakov Bar-Shalom§
Electrical and Systems Engineering Department
University of Connecticut
Storrs CT 06269-2157, USA.

Abstract

The problem of acquiring an incoming theater ballistic missile (TBM) presents many complex challenges. The missile should be detected and its state estimated using the measurements available from a short window of time because the flight time is short. In this paper the acquisition of an incoming tactical ballistic missile using the measurements from a surface based Electronically Scanned Array (ESA) radar is presented. In view of the emergence of low radar cross section TBMs, it is important to be able to acquire low SNR targets at long range. Such targets are characterized by low detection probability and high false alarm rate. We present a batch Maximum Likelihood Estimator (MLE) to acquire the missile while it is exo-atmospheric. The proposed estimator, which combines MLE with the Probabilistic Data Association (PDA) algorithm to handle false alarms/clutter, also uses the amplitude information (signal strength), in addition to range and angle measurements, to obtain accurate target state estimates. The use of the amplitude information facilitates target acquisition under low SNR conditions. Typically, ESA radars operate at around 13dB, whereas the new estimator is shown to be effective even at 4dB SNR, for a Swerling III type fluctuating target, which represents significant counter-stealth capability. In other words, this algorithm acts as an effective "power multiplier" for the radar by a factor of 8 (9dB). In addition to the ML estimator, a track validation scheme, which is used to confirm the presence of an incoming missile at the estimated location, is also presented. The Cramer-Rao Lower Bound, which quantifies the state estimate accuracies attainable for this low-observable estimation problem, is also presented and shown to be achieved by the proposed estimator. It is also shown that the optimum detection threshold of the radar can be found by maximizing the information reduction factor that accounts for the loss of information.

1 Introduction

A substantial threat comes from the theater ballistic missiles (TBM) with range of less than 500 miles. This has stimulated extensive activity in the area of Ballistic Missile Defense (BMD). The first requirement is acquiring and tracking incoming missiles to eventually direct interceptors or other defense apparatus to destroy them. The acquisition of a missile consists of estimating its position and velocity using sensors like radars or electro optical sensors (EOS). Some of the technical challenges that must be overcome are the short time available for acquiring a missile, the need of acquisition at a long range and the presence of spurious measurements due to the low detection threshold made necessary by the

*Research supported by ONR/BMDO grants N00014-91-J-1450, N00014-97-1-0502 and AFOSR grant F409620-97-1-0198.

†Email: *siva@arcon.com.* Research performed while at the University of Connecticut.

‡Email: *kiruba@ee.uconn.edu.*

§Email: *ybs@ee.uconn.edu.*

target's low radar cross section (RCS). Since current systems will typically initiate a track only if there is a signal-to-noise ratio (SNR) of 13 dB , it is of interest to investigate algorithms that can perform this for substantially lower SNR. Specifically, this paper presents an algorithm that can detect a track and initialize it for a fluctuating target with an average SNR of 4 dB. In other words, this algorithm acts as an effective power multiplier for the radar by a factor of 8.

The flight of a ballistic missile consists of three phases, boost phase, ballistic phase (midcourse or free flight phase) and terminal phase (reentry phase). These phases are illustrated in Figure 1. The total flight time lasts for 5-10 minutes. When a missile is launched, early warning satellites can detect the hot exhaust plume of the missile and provide information to surface based radars to search for the missile in a cueing region. This paper deals with the problem of enhancing the performance of the existing surface based radar in detecting and initiating the track before the missile enters the terminal phase.

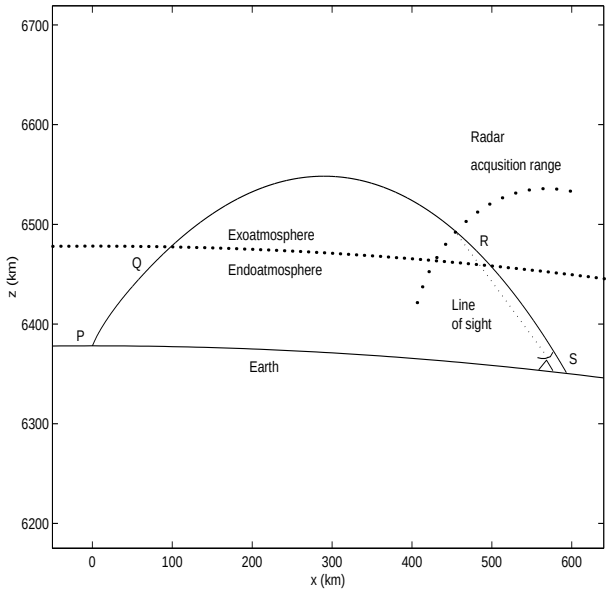

PQ - boost phase, QR - ballistic phase
RS - terminal phase

Figure 1: Stages of ballistic missile trajectory.

There has been a widespread interest to develop tracking algorithms for an effective defense against tactical ballistic missiles. An optimal ballistic missile track initiation algorithm based on Maximum Likelihood (ML) Estimator using midcourse satellite observations is presented by (Yeddanapudi, *et. al.*, 1997). An extensive investigation of the performance of various filters based on extended Kalman filter (EKF) for the reentry phase was done by (Mehra, 1971) and (Siouris, *et. al.*, 1997). One of the main difficulties is to acquire the missiles at a sufficiently early stage. This is important because defense systems should be able to intercept the missile well above the intended impact point. The problem is compounded by the inherent difficulty of detecting the track of low SNR targets due to the unavoidable high false alarm rate with which the tracker has to deal. The related work is (Yi Cong, *et. al.*, 1997) where satellite based infrared (IR) measurements were used to estimate the trajectory of a TBM during boost phase (when it is highly visible once it is above the clouds). Subsequently, this was used to predict the position of the TBM just prior to reentry when it enters the acquisition range of a surface based radar. This will be used in the present work to cue the radar search.

Target detection and tracking in the presence of clutter[1] has been treated extensively in the literature. The work in (Jauffret, *et. al.*, 1990) deals with the problem of track formation in the case of passive sonar systems. However, the ballistic missile acquisition problem demands additional consideration due to the unique difficulties it presents. The equations governing the motion of the target are nonlinear. The extended Kalman filter formulation for this problem would not only have to deal with usual approximations of nonlinearities, but it would require identification of the target-originated measurements, which is not feasible in a low SNR situation. (see, e.g., Fig 5). The work of (Jauffret, *et. al.*, 1996) extended the approach of (Kirubarajan, *et. al.*, 199) by including the amplitude information (AI) of the received signal in the ML estimator to enhance the observability of the target. Incorporation of this information in the likelihood function enables track detection and estimation at very low SNR. Another work (Lerro, *et. al.*, 1993) investigated the performance of the interacting multiple model (IMM) estimator for tracking with target amplitude feature.

This paper is organized as follows. First, some background material is presented in Section 2, along with the model of the radar, model of the target and derivation of the probability distribution function of SNR. Section 3 presents the formulation of the estimator, the underlying statistical assumptions, the bounds of the estimator and the likelihood ratio test, which is used to validate the track. It is also shown that the optimum detection threshold of the radar can be found by maximizing the information reduction factor that accounts for the loss of information. We illustrate the numerical implementation of the estimator in Section 4. Finally, Section 5 summarizes the results.

2 Background

The main focus of this paper is to initialize the missile trajectory state estimate using the measurements obtained by a surface based radar for a short period of time (typically 5s), before it enters the atmosphere. These measurements contain a large number of false detections and the target originated measurements cannot be distinguished from the false measurements. In this paper a ML estimator to estimate the target state at an SNR as low as 4 dB is presented. The ML estimate of an unknown target parameter vector $\mathbf{x}$ is the value of $\mathbf{x}$ which maximizes the conditional density $p(\mathbf{Z}|\mathbf{x})$ of the observation (measurement) vector $\mathbf{Z}$ which is the likelihood function of $\mathbf{x}$ (Bar-Shalom, *et. al.*, 1998). The major features of the approach are:

1. Use of the exact ballistic motion equations of the target,
2. Ability to handle false measurements ($P_{FA} > 0$) and target detection probability $P_D < 1$,
3. Incorporation of target features — in this case the target RCS fluctuation model with a certain average SNR.

2.1 Coordinate Systems and Target Model

The motion of the missile above the atmosphere is governed by Kepler's laws. Three right handed Cartesian coordinate systems having origins at different locations are used in formulating the problem. The earth centered inertial (ECI) coordinate system has its origin at the center of the earth, with the positive x axis pointing along the vernal equinox direction and the positive z axis passing through the North pole. Kepler's laws are expressed in this coordinate system. The earth centered earth fixed (ECEF) coordinate system has its origin at the center of the earth, with the positive x axis passing through the prime meridian at the equator and the positive z axis passing through the North pole. The third coordinate

[1] In most instances, clutter referred to random clutter, which, like the false alarms, can be modeled by a spatial Poisson process.

frame is located at the radar. This frame has its origin at the radar, with the positive x axis pointing towards the north and the positive z axis pointing vertically up. Let $\mathbf{x}_k^{\mathrm{R}} = [\mathbf{p}_k' \ \dot{\mathbf{p}}_k']'$ be the 6 dimensional target state vector at time t_k, where the superscript R denotes that the vector is expressed with respect to radar coordinate frame. The vectors $\mathbf{p}_k = [\xi(t_k) \ \eta(t_k) \ \zeta(t_k)]'$ and $\dot{\mathbf{p}}_k = [\dot{\xi}(t_k) \ \dot{\eta}(t_k) \ \dot{\zeta}(t_k)]'$ are the position and velocity of the target, respectively. The state of the target at the reference time t_0 is $\mathbf{x}_0^{\mathrm{R}}$. The state propagation equation can be represented as

$$\mathbf{x}_k^{\mathrm{R}} = \mathbf{f}(\mathbf{x}_0^{\mathrm{R}}, t_0, t_k) \tag{1}$$

where $\mathbf{f}(\cdot)$ is given in Appendix A.

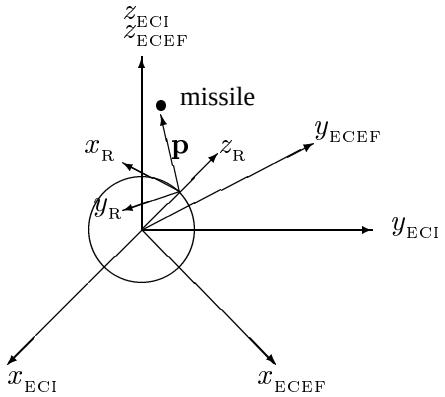

Figure 2: Relative positions of ECI, ECEF and Radar coordinate axes.

2.2 Radar Operation

In the development of the problem a 4 GHz amplitude comparison monopulse phased array radar with uniform illumination across the array is emulated (Blair, *et. al.*, 1998). Each radar dwell consists of one phase/frequency discrete coded pulse. The range gate is assumed to cover the cueing region depth while several beams are needed to cover this region in width. The radar beam is quasi-circular with the 3 dB beamwidth, θ_{bw}, increasing as the beam is steered off the broadside direction. The beam is pointed to the commanded direction given by the radar manager.

In a typical missile acquisition scenario the radar performs a volumetric search scan over the surveillance volume using a number of dwells. This is achieved by changing the commanded direction and the commanded slant range (gate location) for each dwell. The dwells can be arranged into a rectangular lattice of rows and columns or into a triangular lattice structure. These beam packing configurations are illustrated in Fig 3. The distance between the circle centers represents the beam step and the diameter represents the beamwidth (not necessarily the 3 dB beamwidth) at the beam crossover point. The overall probability of detection of a scan depends on the ratio of the beam step to 3 dB beamwidth (Fielding, 1993). The related problem of efficient searching with an agile sensor for a target, assumed stationary, was considered in (Duncan, 1996).

In the case of triangular lattice packing configuration, for example, the probability of detection, P_{d_i}, in the region of the i-th hexagon, which encloses a single dwell as shown in Fig 3(b), is given by

$$P_{d_i} \quad = \quad \frac{1}{m} \sum_{j=1}^{m} P_{d_{ij}} \tag{2}$$

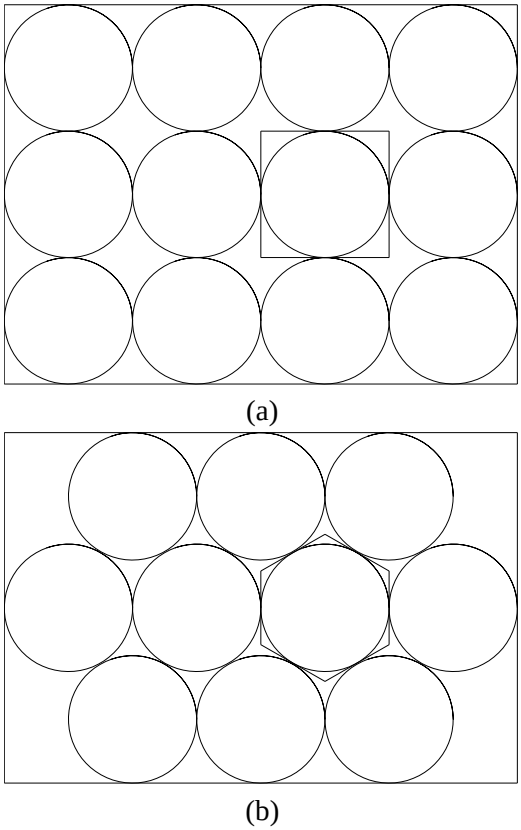

Figure 3: Dwell stacking arrangements in a scan: (a) rectangular lattice; (b) triangular lattice.

where $P_{d_{ij}}$ is the average of probability of detections over the hexagon at j-th bin due to all the dwells in the scan and m is the number of range bins (see Appendix F). The target location is assumed to be uniform in the hexagonal region. The probability of detection P_{d_i} in each of the n hexagons varies due to the (slight) change in radar gain in the beam direction. The overall probability of detection P_D from n hexagons is taken as[2]

$$P_D = \frac{1}{n}\sum_{i=1}^{n} P_{d_i} \tag{3}$$

2.3 Radar Model

This subsection presents the radar model which will be needed in the derivation of the probability density function (pdf) of the SNR in the next subsection. This in turn is needed for the likelihood function that includes the signal strength information. For a radar with a given transmitted power P_t, the SNR of the output of the matched filter at time t_k is given by (Barton, 1964)

$$\Re_k' = \frac{P_t G_t G_r \lambda^2 F_t^2 F_r^2 \delta}{(4\pi)^3 L_{tot}} \left(\frac{\tau_e}{kT_0 F_n}\right) \left(\frac{G_{stc}(r_k)}{r_k^4}\right) \tag{4}$$

where

$$\Re_k' = \text{SNR}$$

[2]Weighted averages based on other distributions can be obtained, but they would make only a small difference.

$$
\begin{aligned}
G_t &= \text{Gain of the transmitter antenna in the direction of the target} \\
G_r &= \text{Gain of the receiver antenna in the direction of the target} \\
\lambda &= \text{Transmit wavelength} \\
F_t &= \text{Transmitter propagation factor} \\
F_r &= \text{Receiver propagation factor} \\
\delta &= \text{Target radar cross section (RCS)} \\
L_{tot} &= \text{Total losses for the radar system} \\
\tau_e &= \text{Pulse width} \\
k &= \text{Boltzmann constant} \\
T_0 &= \text{Reference temperature} \\
F_n &= \text{Receiver noise figure} \\
r_k &= ||\mathbf{p}_k|| = \text{Slant range of the target} \\
G_{stc}(r) &= \text{Sensitivity Time Control (STC) gain}
\end{aligned}
$$

The sensitivity time control gain is

$$
G_{stc}(r_k) = \begin{cases} 1 & r_k \geq r_{stc} \\ \left(\frac{r_k}{r_{stc}}\right)^3 & r_k < r_{stc} \end{cases} \tag{5}
$$

where $r_{stc} = 30$ km is used to avoid saturation of the receiver amplifier when the target is close to the radar. The array radar consists of N^2 individual elements (i.e., N elements in elevation and bearing) with cosine illumination. The broadside of the array is directed at the bearing angle of b_q and elevation angle of e_q. The received voltage will be related to the received power as $V_{rec} = \sqrt{2P_r}$. The received sum voltage S_k at time t_k is composed of the in-phase and quadrature phase voltages. In the case of a noncoherent detection, the noisy in-phase (S_{ik}) and quadrature (S_{qk}) components of the sum voltage normalized by the receiver noise are

$$
S_{ik} = \mathcal{A}_k(\Sigma_k)^2 \cos\phi_k + \mathcal{N}(0,1) \tag{6}
$$

$$
S_{qk} = \mathcal{A}_k(\Sigma_k)^2 \sin\phi_k + \mathcal{N}(0,1) \tag{7}
$$

where $\mathcal{N}(0,1)$ represents a zero-mean unity-variance normal random variable (the normalized noise). Using (4) the normalized amplitude of the received signal $\mathcal{A}_k$ can be expressed as

$$
\mathcal{A}_k = \frac{\mathcal{K}_0}{r_k^2}\sqrt{\delta\, G_{stc}(r_k)} \tag{8}
$$

where

$$
\mathcal{K}_0 = \sqrt{\frac{2P_t G_t G_r F_t^2 F_r^2 \lambda^2 \tau_e}{(4\pi)^3 L_{tot} k T_0 F_n}} \tag{9}
$$

is the received voltage reflected from a unit radar cross section target at unit distance. The resultant two dimensional normalized radiation pattern Σ_k due to simultaneous lobing (Skolnik, 1980) is given by

$$
\begin{aligned}
\Sigma_k = {} & \Psi_k(\theta^e_{sq}, \theta^b_{sq}) + \Psi_k(-\theta^e_{sq}, \theta^b_{sq}) + \\
& \Psi_k(\theta^e_{sq}, -\theta^b_{sq}) + \Psi_k(-\theta^e_{sq}, -\theta^b_{sq})
\end{aligned} \tag{10}
$$

where

$$\begin{aligned}\Psi_k(\theta^e_{sq},\theta^b_{sq}) &= [V_e(\epsilon(\mathbf{x}_k), e_k+\theta^e_{sq})\cdot \\ &\quad V_b(\beta(\mathbf{x}_k), b_k+\theta^b_{sq})]\end{aligned} \tag{11}$$

is the two dimensional normalized radiation pattern of a single lobe and θ^b_{sq} and θ^e_{sq} are the squint angles in bearing and elevation. The angles b_k and e_k in (11) denote the bearing and elevation pointing commands given to the radar and $\beta(\mathbf{x}_k)$ and $\epsilon(\mathbf{x}_k)$ are the bearing and elevation of the target where the superscript of $\mathbf{x}_k$ has been dropped. The squint angles are evaluated using

$$\theta^b_{sq} = \frac{\theta_{sq0}}{\cos(b_k - b_q)} \tag{12}$$

$$\theta^e_{sq} = \frac{\theta_{sq0}}{\cos(e_k - e_q)} \tag{13}$$

where θ_{sq0} is 0.9°. The normalized radiation patterns in bearing $V_b(\beta(\mathbf{x}_k), b_k)$ and elevation $V_e(\epsilon(\mathbf{x}_k), e_k)$ are given by

$$\begin{aligned}V_b(\beta(\mathbf{x}_k), b_k) &= \frac{\pi}{4(1.43)}\frac{\sin(Na_2)}{N\sin(a_2)}\cdot \\ &\quad \left[\frac{\sin(a_1+0.5\pi)}{a1+0.5\pi}+\frac{\sin(a_1-0.5\pi)}{a_1-0.5\pi}\right]\end{aligned} \tag{14}$$

$$\begin{aligned}V_e(\epsilon(\mathbf{x}_k), e_k) &= \frac{\pi}{4(1.43)}\frac{\sin(Nb_2)}{N\sin(b_2)}\cdot \\ &\quad \left[\frac{\sin(b_1+0.5\pi)}{b_1+0.5\pi}+\frac{\sin(b_1-0.5\pi)}{b_1-0.5\pi}\right]\end{aligned} \tag{15}$$

where

$$a_1 = 0.25\sin(\beta(\mathbf{x}_k) - b_q) \tag{16}$$

$$a_2 = 0.5\pi[\sin(\beta(\mathbf{x}_k) - b_q) - \sin(b_k - b_q)] \tag{17}$$

$$b_1 = 0.25\sin(\epsilon(\mathbf{x}_k) - e_q) \tag{18}$$

$$b_2 = 0.5\pi[\sin(\epsilon(\mathbf{x}_k) - e_q) - \sin(e_k - e_q)] \tag{19}$$

The factor of 1.43 has been introduced in (14) and (15) to give a normalized sum channel voltage at boresight for a broadside angle of 0°.

2.4 PDF of SNR

For a Swerling III type target the pdf of the radar cross section δ is given by (Swerling, *et. al.*, 1990)

$$p(\delta) = \frac{4\delta}{\delta_0^2}\exp\left(-\frac{2\delta}{\delta_0}\right) \tag{20}$$

where δ_0 is the average radar cross section of the target. Using (8) it can be shown that, for a target at a given distance r_k, $\mathcal{A}_k$ has the pdf

$$p(\mathcal{A}_k|\mathbf{x}_k) = \frac{8\mathcal{A}_k^3}{\alpha_k^2}\exp\left(-\frac{2\mathcal{A}_k^2}{\alpha_k}\right) \tag{21}$$

where

$$\alpha_k \;=\; \frac{\mathcal{K}_o^2\, G_{stc}(r_k)}{r_k^4}\,\delta_0 \tag{22}$$

the signal power without the radar off-boresight-attenuation, is a function of the target's average radar cross section δ_0 and slant range r_k, which in turn is a function of the target position vector $\mathbf{p}_k$. From (6) and (7) the pdf of S_{ik} and S_{qk} can be written as

$$p(S_{ik}|\mathcal{A}_k, \mathbf{x}_k, \phi) \;=\; \mathcal{N}(\mathcal{A}_k\Sigma_k^2\cos\phi, 1) \tag{23}$$

$$p(S_{qk}|\mathcal{A}_k, \mathbf{x}_k, \phi) \;=\; \mathcal{N}(\mathcal{A}_k\Sigma_k^2\sin\phi, 1) \tag{24}$$

where Σ_k is a function of target position vector $\mathbf{p}_k$ and is obtained from (10)–(19). The amplitude of the received signal, S_k, (actually, signal + noise — see (6),(7)) is given by

$$S_k^2 \;=\; S_{ik}^2 + S_{qk}^2 \tag{25}$$

The pdf of S_k can be shown to be (Bossé, *et. al.*, 1991)

$$p(S_k|\mathcal{A}_k, \mathbf{x}_k) \;=\; S_k\,\exp\left\{-\frac{S_k^2+\mathcal{A}_k^2\Sigma_k^4}{2}\right\}\cdot I_0(\mathcal{A}_k\Sigma_k^2 S_k) \tag{26}$$

where $I_0(\cdot)$ is the modified Bessel function of the first kind of order zero. Since the SNR (actually, signal-plus-noise to noise ratio) $\Re_k = \frac{1}{2}S_k^2$, the pdf of $\Re_k$ can be written as

$$p(\Re_k|\mathcal{A}_k, \mathbf{x}_k) \;=\; \exp\left\{-\left(\Re_k+\frac{\mathcal{A}_k^2\Sigma_k^4}{2}\right)\right\}\cdot I_0(\mathcal{A}_k\Sigma_k^2\sqrt{2\Re_k}) \tag{27}$$

The pdf of the SNR conditioned on the target state can be expressed as

$$\begin{aligned} p(\Re_k|\mathbf{x}_k) \;&=\; \int_0^\infty p(\Re|\mathcal{A}_k,\mathbf{x})p(\mathcal{A}_k|\mathbf{x})\,d\mathcal{A}_k \\ &=\; \frac{8e^{-\Re}}{\alpha_k^2}\int_0^\infty \exp\left\{-\left(\frac{2}{\alpha_k}+\frac{\Sigma_k^4}{2}\right)\mathcal{A}_k^2\right\}\cdot \\ &\quad I_0(\mathcal{A}_k\Sigma_k^2\sqrt{2\Re})\mathcal{A}_k^3\,d\mathcal{A}_k \end{aligned} \tag{28}$$

The integral on the right hand side of (28) is given by (Watson, 1994) as

$$\begin{aligned} \int_0^\infty t^{\mu-1}\exp(-t^2p^2)I_\nu(qt)\,dt \;&=\; \frac{\Gamma\left(\frac{\mu+\nu}{2}\right)\left(\frac{q}{2p}\right)^\nu}{2p^\mu\Gamma(\nu+1)}\cdot \\ &\quad \exp\left(\frac{q^2}{4p^2}\right)\,{}_1F_1\left(\frac{\nu-\mu}{2}+1;\nu+1;-\frac{q^2}{4p^2}\right) \end{aligned} \tag{29}$$

where ${}_1F_1(c;d;y)$ is a confluent hypergeometric function (Watson, 1994) which can be expanded as

$$\begin{aligned} {}_1F_1(c;d;y) \;&=\; 1+\frac{c}{1!d}y+\frac{c(c+1)}{2!d(d+1)}y^2+ \\ &\quad \frac{c(c+1)(c+2)}{3!d(d+1)(d+2)}y^3.... \end{aligned} \tag{30}$$

In this case $c = -1, d = 1, y = -q^2/4p^2$ and the series representation terminates after the first two terms. Finally, the pdf of the SNR of a target measurement is obtained as

$$p_1(\Re_k|\mathbf{x}_k) = \frac{16}{(4+\alpha_k\Sigma_k^4)^2}\exp\left(-\Re_k + \frac{\alpha_k\Sigma_k^4\Re_k}{4+\alpha_k\Sigma_k^4}\right)\cdot \left(1+\frac{\alpha_k\Sigma_k^4\Re_k}{4+\alpha_k\Sigma_k^4}\right) \tag{31}$$

where $\alpha_k\Sigma_k^4$ is twice the effective average SNR (actually, signal-plus-noise to noise ratio, including the radar radiation pattern effect – i.e., the reduction Σ_k due to the target being off the beam boresight). The expected value of $\Re_k$, given the target state $\mathbf{x}_k$, is $1+\alpha_k\Sigma_k^4/2$. In the case of false alarms the pdf of S_k will be given by

$$p_0(S_k) = S_k\exp\left(-\frac{S_k^2}{2}\right) \tag{32}$$

In reality the distributions of clutter exhibit both higher tails and larger standard deviation-to-mean ratio than the Rayleigh density of (32) (Conte, *et. al.*, 1991). A better fit can be achieved by resorting to a Weibull distribution. The influence on the performance of the radar due to the mismatch of clutter densities can be found in (Conte, *et. al.*, 1994). To conform with (Blair, *et. al.*, 1998) we will continue to use (32).

The pdf of the SNR if the measurement is false (due to noise only — average is unity) is

$$p_0(\Re_k) = \exp(-\Re_k) \tag{33}$$

The measurements whose SNR exceed the threshold set by the operator will be accepted by the radar as valid measurements. The operator will decide the threshold τ using the probability of false alarm P_{FA} which is to be maintained. The threshold τ follows from

$$P_{FA} = \int_\tau^\infty e^{-\Re}\,d\Re \tag{34}$$

Thus, the pdf of the SNR of a false measurement that exceeded the threshold τ is

$$p_0^\tau(\Re_k) = \frac{1}{P_{FA}}e^{-\Re_k} \qquad \Re_k > \tau \tag{35}$$

From the threshold, the probability of detection ($P_{d_{ij}}$) of a measurement in the jth range bin of ith dwell can be calculated using

$$P_{d_{ij}} = \frac{16}{(4+\alpha_k\Sigma_k^4)^2}\int_\tau^\infty \exp\left(-\Re + \frac{\alpha_k\Sigma_k^4\Re}{4+\alpha_k\Sigma_k^4}\right)\cdot \left(1+\frac{\alpha_k\Sigma_k^4\Re}{4+\alpha_k\Sigma_k^4}\right)d\Re \tag{36}$$

The pdf of the SNR of a target originated measurement that exceeded the threshold τ is

$$p_1^\tau(\Re_k|\mathbf{x}_k) = \frac{16}{P_D(4+\alpha_k\Sigma_k^4)^2}\exp\left(-\Re + \frac{\alpha_k\Sigma_k^4\Re}{4+\alpha_k\Sigma_k^4}\right)\cdot \left(1+\frac{\alpha_k\Sigma_k^4\Re}{4+\alpha_k\Sigma_k^4}\right) \qquad \Re_k > \tau \tag{37}$$

where P_D is given by (3).

3 Maximum Likelihood Estimator

3.1 The Likelihood Ratio

We now derive the maximum likelihood estimator, which is used in conjunction with the Probabilistic Data Association (PDA) algorithm. It is assumed that N sets of measurements are made at times $t_i, i = 1, 2, \ldots N$ where the index denotes the scan number. The kth measurement in the ith scan is defined by the vector

$$z_{ik} \quad = \quad [\Re_{ik}\ r_{ik}\ \beta_{ik}\ \epsilon_{ik}]' \tag{38}$$

where $\Re_{ik},\ r_{ik},\ \theta_{ik}$ and β_{ik} are SNR, slant range, bearing, elevation, respectively. The radar performs a volumetric search over the region of interest (cueing region) obtained from prior information, e.g., as shown in (Yeddanapudi, *et. al.*, 1997) and (Yi Cong, *et. al.*, 1997). It is also assumed that all the dwells in a scan are made at (practically) the same time. Let there be m_i measurements (detection threshold exceedances) in the ith scan made at time t_i. This set is denoted by

$$Z(i) \quad = \quad \{z_{ik}\}_{k=1}^{m_i} \tag{39}$$

The cumulative set of measurements during the entire period is

$$\mathbf{Z} \quad = \quad \{Z(i)\}_{i=1}^{N} \tag{40}$$

where N is the total number of scans. In addition to the above, the following assumptions about the statistical characteristics of the measurements are also made.

1. The measurements at two different scans are conditionally independent.

$$p[Z(i), Z(j)|\mathbf{x}] \quad = \quad p[Z(i)|\mathbf{x}]p[Z(j)|\mathbf{x}] \tag{41}$$

2. A measurement that originated from the target at a particular scan is received by the radar only once during the scan with probability P_D and is corrupted by zero mean Gaussian noise. That is

$$r_{ik} \quad = \quad r_i(\mathbf{x}) + w_{ik}^r \tag{42}$$
$$\beta_{ik} \quad = \quad \beta_i(\mathbf{x}) + w_{ik}^\beta \tag{43}$$
$$\epsilon_{ik} \quad = \quad \epsilon_i(\mathbf{x}) + w_{ik}^\epsilon \tag{44}$$

   where $w_{ik}^r,\ w_{ik}^\beta,\ w_{ik}^\epsilon$ are the measurement noise components with standard deviations σ^r, σ_{ik}^β, and σ_{ik}^ϵ respectively.

3. In the case of a false alarm the slant range measurement is distributed uniformly in the range gate, and bearing and elevation are Gaussian distributed around the commanded bearing b_{ik} and elevation e_{ik} (beam boresight) respectively.[3] That is

$$r_{ik} \quad \sim \quad \mathcal{U}[R_1,\ R_2] \tag{45}$$
$$\beta_{ik} \quad \sim \quad \mathcal{N}(b_{ik}, (\sigma_{ik}^\beta)^2) \tag{46}$$
$$\epsilon_{ik} \quad \sim \quad \mathcal{N}(e_{ik}, (\sigma_{ik}^\epsilon)^2) \tag{47}$$

   where R_1 and R_2 are the lower and upper limits of the range gate respectively.

[3]This is based on the radar emulator (Blair, *et. al.*, 1998). This is different from the model used in (Kirubarajan, *et. al.*, 1996) where the false measurements were uniformly distributed in the entire measurement space. The central tendency of the false measurements in angle about the beam boresight is a consequence of the fact that the monopulse ratio (Blair, *et. al.*, 1998) when there is noise only is zero mean and is unlikely to assume large values.

4. The number of false measurements in a volume v at a sampling instant obeys a Poisson probability mass function (pmf) with a known expected number of false measurements λ per unit volume,

$$\mu(m_i) = \frac{e^{-\lambda v}(\lambda v)^{m_i}}{m_i!} \tag{48}$$

The parameter λ is determined by the detection threshold and is given by P_{FA} multiplied by the volume of a resolution cell. Each resolution cell is a range cell in a beam.

If there are m_i measurements in the ith scan, the mutually exclusive and exhaustive events giving rise to these measurements are

$$\varepsilon_k(i) = \begin{cases} \text{all measurements are false} \\ k = 0 \\ \text{measurement } z_{ik} \text{ is from the target} \\ k = 1, \ldots, m_i \end{cases} \tag{49}$$

The pdf of the measurements corresponding to the above events can be written as

$$p_0(Z(i)|\varepsilon_0(i)) = \prod_{j=1}^{m_i} p_0^{\tau}(\Re_{ij}) p_0(r_{ij}) p_0(\beta_{ij}) p_0(\epsilon_{ij}) \qquad k = 0 \tag{50}$$

$$p_1(Z(i)|\mathbf{x}, \varepsilon_k(i)) = p_1^{\tau}(\Re_{ik}|\mathbf{x}) p_1(r_{ik}|\mathbf{x}) p_1(\beta_{ik}|\mathbf{x}) \cdot p_1(\epsilon_{ik}|\mathbf{x}) \prod_{j=1, j\neq k}^{m_i} p_0^{\tau}(\Re_{ij}) p_0(r_{ij}) p_0(\beta_{ij}) p_0(\epsilon_{ij}) \qquad k = 1, \ldots, m_i \tag{51}$$

where $\mathbf{x}$ denotes the state of the target (at the reference time).

Let

$$\rho_{ik} = \frac{p_1^{\tau}(\Re_{ik}|\mathbf{x})}{p_0^{\tau}(\Re_{ik})} = \theta_{ik}(1 + \nu_{ik}\Re_{ik}) e^{\nu_{ik}\Re_{ik}} \tag{52}$$

and

$$\frac{p_1(r_{ik}|\mathbf{x}) p_1(\beta_{ik}|\mathbf{x}) p_1(\epsilon_{ik}|\mathbf{x})}{p_0(r_{ik}) p_0(\beta_{ik}) p_0(\epsilon_{ik})} = \frac{v_r}{\sqrt{2\pi}\sigma^r} \cdot \exp\left(\psi(z_{ik}, \mathbf{x})\right) \tag{53}$$

where

$$\theta_{ik} = \frac{16\, P_{FA}}{P_D(4 + \alpha_{ik}\Sigma_{ik}^4)^2} \tag{54}$$

$$\nu_{ik} = \frac{\alpha_{ik}\Sigma_{ik}^4}{4 + \alpha_{ik}\Sigma_{ik}^4} \tag{55}$$

$$\psi(z_{ik}, \mathbf{x}) = -\frac{(r_{ik} - r_i(\mathbf{x}))^2}{2(\sigma^r)^2} - \frac{(\beta_{ik} - \beta_i(\mathbf{x}))^2}{2(\sigma_{ik}^{\beta})^2} + \frac{(\beta_{ik} - b_{ik})^2}{2(\sigma_{ik}^{\beta})^2} - \frac{(\epsilon_{ik} - \epsilon_i(\mathbf{x}))^2}{2(\sigma_{ik}^{\epsilon})^2} + \frac{(\epsilon_{ik} - e_{ik})^2}{2(\sigma_{ik}^{\epsilon})^2} \tag{56}$$

and v_r is the range gate length. Using the total probability theorem the pdf of the set of measurements at t_i can be written as (Kirubarajan, *et. al.*, 1996)

$$\begin{aligned} p[Z(i)|\mathbf{x}] &= \frac{\mu(m_i)}{c_i} \prod_{j=1}^{m_i} p_0^{\tau}(\Re_{ij}) p_0(r_{ij}) p_0(\beta_{ij}) p_0(\epsilon_{ij}) \cdot \\ & \left\{ \frac{\mu(m_i - 1) P_D v_r}{m_i \mu(m_i)} \sum_{k=1}^{m_i} \frac{\rho_{ik}}{\sqrt{2\pi}\sigma^r} \exp(\psi(z_{ik}, \mathbf{x})) + (1 - P_D) \right\} \end{aligned} \tag{57}$$

where c_i is a normalization factor given by

$$c_i = (1 - P_D)\mu(m_i) + P_D \mu(m_i - 1) \tag{58}$$

The dimensionless likelihood ratio is obtained by dividing the above equation by $p[Z(i)|\varepsilon_0(i)]$, namely,

$$\begin{aligned} \Phi(Z(i), \mathbf{x}) &= \frac{p(Z(i)|\mathbf{x})}{p(Z(i)|\varepsilon_0(i))} \\ &= \frac{1}{c_i} \left\{ \frac{P_D \mu(m_i - 1) v_r}{m_i \, \mu(m_i)} \sum_{k=1}^{m_i} \frac{\rho_{ik}}{\sqrt{2\pi}\sigma^r} \right. \\ &\quad \left. \exp(\psi(z_{ik}, \mathbf{x})) + (1 - P_D) \right\} \\ &= \frac{1}{c_i} \left\{ \frac{P_D}{\lambda_r} \sum_{k=1}^{m} \frac{\rho_{ik}}{\sqrt{2\pi}\sigma^r} \exp(\psi(z_{ik}, \mathbf{x})) + \right. \\ &\quad \left. (1 - P_D) \right\} \end{aligned} \tag{59}$$

where λ_r is the expected number of false alarms per unit distance in range. Using the conditional independence of measurements, the pdf of the entire set of measurements — the global likelihood function of $\mathbf{x}$ — can be written as

$$p[\mathbf{Z}|\mathbf{x}] = \prod_{i=1}^{N} p[Z(i)|\mathbf{x}] \tag{60}$$

Subsequently the dimensionless likelihood ratio using the entire set of measurements is given by

$$\Phi[\mathbf{Z}, \mathbf{x}] = \prod_{i=1}^{N} \Phi[Z(i), \mathbf{x}] \tag{61}$$

Then the log-likelihood ratio is

$$\begin{aligned} \phi[\mathbf{Z}, \mathbf{x}] &= \ln(\phi[\mathbf{Z}, \mathbf{x}]) \\ &= \sum_{i=1}^{N} \ln \left\{ \frac{P_D}{\lambda_r} \sum_{k=1}^{m_i} \frac{\rho_k}{\sqrt{2\pi}\sigma^r} \exp(\psi(z_k, \mathbf{x})) + \right. \\ &\quad \left. (1 - P_D) \right\} - \sum_{i=1}^{N} \ln\{c_i\} \end{aligned} \tag{62}$$

In the above equation the second summation involving c_i can be omitted when finding the maximum likelihood estimate since it does not depend on $\mathbf{x}$. The use of the global likelihood function (60) is the key to obtain the power multiplier feature, as will be seen later.

3.2 Numerical Calculation of Maximum Likelihood Estimate

The maximization of the log-likelihood ratio is done using the quasi-Newton (variable metric) method. This can equivalently be done by minimizing the negative log-likelihood ratio. In variable metric method the objective function $f(x)$ is approximated as a quadratic form around the current estimate $\mathbf{x}_q$.

$$\begin{aligned} f(\mathbf{x}) &= f(\mathbf{x}_q) + (\mathbf{x}-\mathbf{x}_q)\nabla f(\mathbf{x}_q) + \\ &\quad \frac{1}{2}(\mathbf{x}-\mathbf{x}_q)A(\mathbf{x}-\mathbf{x}_q) \end{aligned} \tag{63}$$

where A is the matrix of second partial derivatives. Then

$$\nabla f(\mathbf{x}) = \nabla f(\mathbf{x}_q) + A(\mathbf{x}-\mathbf{x}_q) \tag{64}$$

The minimum point is determined by setting $\nabla f(\mathbf{x}) = 0$, which yields

$$\mathbf{x}-\mathbf{x}_q = A^{-1}\nabla f(\mathbf{x}_q) \tag{65}$$

The left hand side is the finite step to get to the exact minimum. This step can be performed if an accurate inverse Hessian $H \approx A^{-1}$ is available. The basic idea of the variable metric method is to build up iteratively a good approximation to the inverse Hessian matrix. That is one needs to construct a sequence of matrices H_q such that

$$\lim_{q\to\infty} H_q = H \tag{66}$$

The procedure is initialized with a positive definite, symmetric approximation to A (usually the identity matrix) and successive H_q's are obtained such that they remain positive definite and symmetric. Far from the minimum, this guarantees that one will always move in a downhill direction (Press, *et. al.*, 1992). Close to the minimum, H_q approaches the true Hessian.

The negative log-likelihood ratio may have many local minima. Due to this the minimization procedure may end up converging to a local minimum instead of the global one. A multipass approach is used to avoid the convergence to a local minimum (Jauffret, *et. al.*, 1990). The idea is to start with a modified negative log-likelihood ratio and minimize it over several passes before solving the exact problem in the last pass. The estimate from one pass is used as the initial estimate for the next. The negative log-likelihood ratio, which is minimized in the p^{th} pass, is modified as

$$\begin{aligned} -\phi[Z^N,\mathbf{x}] &= -\sum_{i=1}^{N} \ln\left\{ \frac{P_D}{\lambda_r} \sum_{k=1}^{m_i} \frac{\rho_{ik}}{\sqrt{2\pi}\sigma^r} \cdot \right. \\ &\quad \left. \exp(\psi(z_{ik},\mathbf{x},p)) + (1-P_D) \right\} + c(\mathbf{x}) \end{aligned} \tag{67}$$

where

$$c(\mathbf{x}) = -\frac{1}{2}\left[\frac{(r(\mathbf{x})-\bar{r})^2}{\sigma_r^2} + \frac{(v(\mathbf{x})-\bar{v})^2}{\sigma_v^2} \right] \tag{68}$$

$v(\mathbf{x}) = ||\dot{\mathbf{p}}||$, $\bar{r}$ is the typical slant range of the target, $\bar{v}$ is the typical speed of the target and σ_r, σ_v are the standard deviations of typical slant range and typical speed respectively. The function $\psi(z_{ik},\mathbf{x},p)$ is written as

$$\begin{aligned} \psi(z_{ik},\mathbf{x},p) &= -\frac{(r_{ik}-r_i(\mathbf{x}))^2}{2(\sigma^r a_p)^2} - \frac{(\beta_{ik}-\beta_i(\mathbf{x}))^2}{2(\sigma_{ik}^{\beta} a_p)^2} + \\ &\quad \frac{(\beta_k - b_{ik})^2}{2(\sigma_{ik}^{\beta} a_p)^2} - \frac{(\epsilon_{ik}-\epsilon_i(\mathbf{x}))^2}{2(\sigma_{ik}^{\epsilon} a_p)^2} + \frac{(\epsilon_{ik}-e_{ik})^2}{2(\sigma_{ik}^{\epsilon} a_p)^2} \end{aligned} \tag{69}$$

The modifying function $c(\mathbf{x})$ is used only in the first $P-1$ passes of the P passes and is set to zero at $p = P$. Also a_p satisfies $a_{p+1} < a_p$ for $p = 1, 2, \ldots P-1$ and $a_P = 1$. This approach prevents the maximization procedure from converging to an unrealistic local maximum and gives a broader view to the estimator. A rough grid search is performed to automatically obtain the initial value for the vector $\mathbf{x}$ for the first pass.

3.3 Cramer-Rao Lower Bound of the Estimator

The Cramer-Rao lower bound (CRLB) is the minimum value of the variance that can be achieved by an unbiased estimator. The ML estimator is said to be efficient if its covariance meets the CRLB. If an ML estimator exists, it is theoretically guaranteed to achieve its CRLB asymptotically. The CRLB of an unbiased ML estimator is

$$E[(\mathbf{x} - \hat{\mathbf{x}})(\mathbf{x} - \hat{\mathbf{x}})] \quge J^{-1} \tag{70}$$

The expectation $E[\cdot]$ in the above equation is over the measurements $\mathbf{Z}$ and J is the Fisher Information Matrix (FIM) given by

$$\begin{aligned} J &= E\{[\nabla_{\mathbf{x}} \ln[p(Z^N|\mathbf{x})]] \cdot \\ &\quad [\nabla_{\mathbf{x}} \ln[p(Z^N|\mathbf{x})]]\}|_{\mathbf{x}=\mathbf{x}^{\text{true}}} \end{aligned} \tag{71}$$

The mutual independence of the measurements also implies that the Fisher information due to the different measurements is additive. In practice, since one does not have the true state of the target, the FIM is evaluated at the estimate. As explained in Appendix C, the FIM J for the missile track initiation problem considered can be written as

$$\begin{aligned} J &= q(P_D, \lambda_g v_g, g, \alpha\Sigma^4) \cdot \\ &\quad \sum_{i=1}^{N} \Bigg(\frac{1}{(\sigma^r)^2} [\nabla_{\mathbf{x}} r_i(\mathbf{x})][\nabla_{\mathbf{x}} r_i(\mathbf{x})]' \\ &\quad + \frac{1}{(\sigma^\beta)^2} [\nabla_{\mathbf{x}} \beta_i(\mathbf{x})][\nabla_{\mathbf{x}} \beta_i(\mathbf{x})]' + \\ &\quad \frac{1}{(\sigma^\epsilon)^2} [\nabla_{\mathbf{x}} \epsilon_i(\mathbf{x})][\nabla_{\mathbf{x}} \epsilon_i(\mathbf{x})]' \Bigg) \end{aligned} \tag{72}$$

where $q(P_D, \lambda_g v_g, g, \alpha\Sigma^4)$ is the information reduction factor that accounts for the loss of information due to the presence of false alarms and the less-than-unity probability of detection (Bar-Shalom, *et. al.*, 1995). Only the measurements which fall within the "validation volume" v_g are considered in deriving (72), where the validation volume (g-sigma region) is

$$v_g = 8\sigma^r \sigma^\beta \sigma^\epsilon g^3 \tag{73}$$

That is, the measurement z_{ik} is considered only if it satisfies the following conditions.

$$\left| \frac{r_{ik} - r_i(\mathbf{x})}{\sigma^r} \right| \leq g \tag{74}$$

$$\left| \frac{\beta_{ik} - \beta_i(\mathbf{x})}{\sigma^\beta} \right| \leq g \tag{75}$$

$$\left| \frac{\epsilon_{ik} - \epsilon_i(\mathbf{x})}{\sigma^\epsilon} \right| \leq g \tag{76}$$

The information reduction factor $q(P_D, \lambda_g v_g, g, \alpha\Sigma^4)$ is given by

$$q(P_D, \lambda_g v_g, g, \alpha\Sigma^4) = \sum_{m=1}^{\infty} \frac{2^6\, \mu(m_i - 1) P_{FA}^{1-m_i}}{\pi\sqrt{2\pi}\, g^{3m_i-3}(4+\alpha\Sigma^4)^2} \cdot I_2(m_i, P_D, \lambda_g v_g, \alpha\Sigma^4) \quad (77)$$

where $I_2(m_i, P_D, \lambda_g v_g, \alpha\Sigma^4)$ is a $4m$ fold integral given in Appendix C.

The rationale for the terminology information reduction factor can be seen by noting that the FIM for zero false alarm probability and unity target detection probability,J_0 is given by (Bar-Shalom, *et. al.*, 1998)

$$J_0 = \sum_{i=1}^{N} \left(\frac{1}{(\sigma^r)^2} [\nabla_{\mathbf{x}} r_i(\mathbf{x})][\nabla_{\mathbf{x}} r_i(\mathbf{x})]' + \frac{1}{(\sigma^\beta)^2} [\nabla_{\mathbf{x}} \beta_i(\mathbf{x})][\nabla_{\mathbf{x}} \beta_i(\mathbf{x})]' + \frac{1}{(\sigma^\epsilon)^2} [\nabla_{\mathbf{x}} \epsilon_i(\mathbf{x})][\nabla_{\mathbf{x}} \epsilon_i(\mathbf{x})]' \right) \quad (78)$$

From (72) and (78) it is clear that $q(P_D, \lambda_g v_g, g, \alpha\Sigma^4)$, which is always less than or equal to unity, represents the loss of information due to clutter and less-than-unity probability of detection. The numerical values of $q(\cdot)$ for different values of detection thresholds and fixed values of g and SNR are presented in Appendix C. The optimum value of the detection threshold can be obtained by choosing the threshold which gives the maximum value of $q(\cdot)$.

In deriving (72) it is assumed that the bearing and elevation measurements are distributed uniformly in the validation region around the commanded bearing and elevation directions respectively. Although a tighter bound can be obtained by using the exact Gaussian distribution for these measurements the derivation of CRLB will be intractable.

3.4 Acceptance of the Estimate

The estimate $\hat{\mathbf{x}}$ obtained by maximizing the log-likelihood ratio (or minimizing the negative log-likelihood ratio) is tested whether it can be accepted as a valid track. This test is performed in order to ensure that the maximization procedure does not converge to a local maximum instead of the global one. Convergence to a local maximum is always possible since the likelihood ratio is multimodal due to the presence of clutter. A test is constructed to distinguish between the following two hypotheses.

$$H_1 = \text{There is one track corresponding to an existing target with a maximum } \hat{\mathbf{x}} \quad (79)$$

$$H_0 = \text{There is no track} \quad (80)$$

According to the Neyman-Pearson Lemma (Poor, *et. al.*, 1994), the uniformly most powerful test of H_1 against H_0 is to consider the dimensionless likelihood ratio $\Phi(\mathbf{Z}, \mathbf{x})$ given in (61) or equivalently, the log-likelihood ratio $\phi(\mathbf{Z}, \mathbf{x})$ given by (62). However, the statistical distribution of $\phi(\mathbf{Z}, \mathbf{x})$ is unknown. The possible approximation is to assume that the central limit theorem holds such that $\phi(\mathbf{Z}, \mathbf{x})$ can be approximated by a Gaussian distribution. Then a test statistic can be defined as (Poor, *et. al.*, 1994)

$$\Lambda = \frac{\phi(\mathbf{Z}, \hat{\mathbf{x}}) - E\{\phi(\mathbf{Z}, \hat{\mathbf{x}}) | H_1\}}{\sqrt{\text{Var}\{\phi(\mathbf{Z}, \hat{\mathbf{x}}) | H_1\}}} \quad (81)$$

Since $\hat{\mathbf{x}}$ is the global maximum under H_1 the following approximations are made:

$$E\{\phi(\mathbf{Z},\hat{\mathbf{x}})|H_1\} \approx E\{\phi(\mathbf{Z},\mathbf{x}^{\text{true}})|H_1\} \quad (82)$$

$$\text{Var}\{\phi(\mathbf{Z},\hat{\mathbf{x}})|H_1\} \approx \text{Var}\{\phi(\mathbf{Z},\mathbf{x}^{\text{true}})|H_1\} \quad (83)$$

Defining the quantities

$$\mu_1 = E\{\phi(Z(i),\mathbf{x}^{\text{true}})|H_1\} \quad (84)$$

$$\sigma_1^2 = \text{Var}\{\phi(Z(i),\mathbf{x}^{\text{true}})|H_1\} \quad (85)$$

the statistic in (81) can be written as

$$\Lambda = \frac{\sum_{i=1}^{N}\phi(Z(i),\hat{\mathbf{x}}) - N\mu_1}{\sqrt{N}\sigma_1} \quad (86)$$

The derivation of the first and second moments of the likelihood ratio to obtain μ_1 and σ_1 are presented in Appendix D. The test for track acceptance is

$$\Lambda \begin{cases} \geq \tau_1 & \text{accept } H_1 \\ < \tau_1 & \text{accept } H_0 \end{cases} \quad (87)$$

According to the assumptions, the test statistic has a zero mean, unity variance Gaussian distribution. Therefore the acquisition probability of the track for a given threshold τ_1 is

$$P_{\text{ACQ}} = P\{\Lambda \geq \tau_1|H_1\} \quad (88)$$

Then, for a given acquisition probability of the track, τ_1 can be calculated using the standard Gaussian. That is

$$P_{\text{ACQ}} = 1 - \frac{1}{\sqrt{2\pi}}\int_{-\infty}^{\tau_1} e^{-\frac{y^2}{2}}dy \quad (89)$$

The false acquisition probability is

$$P_{\text{FACQ}} = P\{\text{accept } H_1|H_0\} = P\{\Lambda > \tau_1|H_0\} \quad (90)$$

Similarly, for the condition where there is no target one can define,

$$\mu_0 = E\{\phi(Z(i))|H_0\} \quad (91)$$

$$\sigma_0^2 = \text{Var}\{\phi(Z(i))|H_0\} \quad (92)$$

Using (91) and (92) as the moments of $\phi(\mathbf{Z},\mathbf{x})$ in (81) and its (assumed) Gaussian distribution, one can obtain a theoretical probability of false track acquisition P_{FACQ}. However, this relies on the tails of the (assumed) Gaussian and is not reliable, in our opinion (the numerical results in (Kirubarajan, *et. al.*, 1996) yielded P_{FACQ} of the order of 10^{-10}). In view of this, we believe that the best indication of the algorithm's false track rejection capability can be obtained via a large number of Monte Carlo runs without a target.

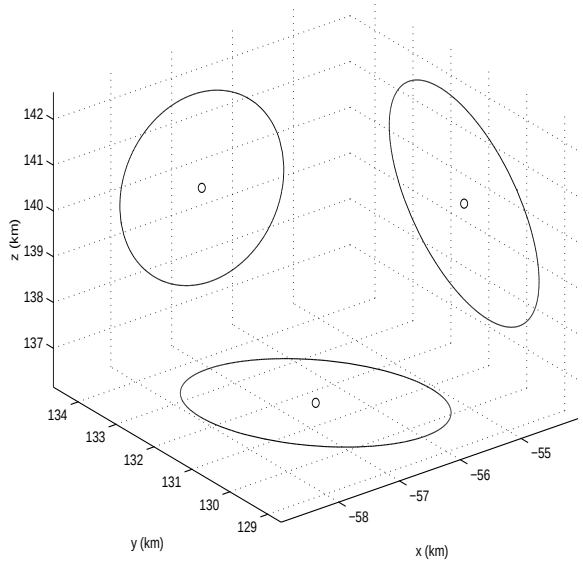

(a)

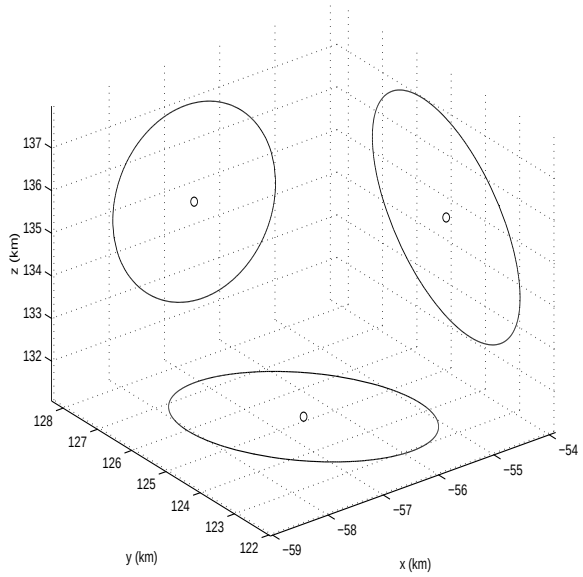

(b)

Figure 4: The 95% probability regions based on the CRLB around the true position of the missile. (a) initial; (b) final

Parameter	Value
P_t	1 MW
N	55
τ_e	675 μs
G_t, G_r	4752
λ	7.5 cm
F_t, F_r	1
L_{tot}	144.5
k	1.38×10^{-23} J/K
T_0	290 K
F_n	2

Table 1: Radar parameters

4 Results

In this section we consider a sample scenario to illustrate the operation of ML/PDA estimator under low SNR conditions. Simulation results were obtained using 100 Monte Carlo runs with the following scenario: the missile enters the radar acquisition region at $t = 0$s with $\mathbf{p}_0^{\text{true}} = [-56.5\ 131.6\ 139.3]'$ km and $\dot{\mathbf{p}}_0^{\text{true}} = [6.7\ \ -155.7\ 770.9]'$ m/s in the radar coordinate frame (see Section 2.1). At this point the radar to target slant range is 200 km. Figures 4(a) and (b) show the initial and final position of the target and the 95% probability regions for the estimates based on the CRLB.

It is assumed that the radar cueing region for initial radar pointing is available from prior information (Yi Cong, *et. al.*, 1997). Then a volumetric search is performed by directing the radar dwells to this region. The radar cueing volume is approximately $(30$ km$)^3$. The average radar cross section of the target being searched is 0.15 m^2. The beamwidth of the radar is 1.6° and the range gate of a dwell consists of 330 bins of length 90m. The parameters of the emulated radar are presented in Table 4. The broadside of the array is directed at 90° bearing and 45° elevation. The above combination of target and radar parameters results in an average target SNNR of 5.4 dB. The detection threshold of the radar is 5.1 dB (this corresponds to $\tau = 3.25$ in (34)) which yields a false alarm probability of 0.0388 per range cell in a beam. The optimum value of the detection threshold τ considering the information reduction factor presented in Table 3 (Appendix C) is 3.14. However, the accuracy of the results is not affected by operating at this slightly suboptimal detection threshold of 5.1 dB since the information reduction factor does not vary significantly between these two detection thresholds. The scans are made at 10 Hz for 6 s. The dwells are stacked in a triangular lattice arrangement as shown in Figure 3(b). The ratio of beamstep to 3 dB beamwidth is maintained at 1.0 so that the radar has a probability of detection (calculated from (36),(2),(3)) of 0.55 for a Swerling III type target with average radar cross section of 0.15 m^2 at 200 km slant range. To cover the cueing region it requires that there be 19 dwells in each scan. Figures 5(a)–(d) present the set of slant range, azimuth, elevation and SNR measurements respectively in one run of the Monte Carlo simulations. It can be seen that target originated measurements are detected about 30 times in 60 scans.[4]

The expected number of false alarms per unit distance can be calculated as

$$\lambda_r \quad = \quad \frac{P_{FA}}{\text{length of range bin}}$$

[4]It should be noted that target can be detected more than once in a scan due to multiple dwells and side-lobe detections. These extra side-lobe target detections are treated as false alarms by the estimator.

$$= \frac{P_{FA}}{90}$$
$$= 3.2 \times 10^{-4}/m \quad (93)$$

From this the expected number of false alarms in a dwell (with the range dimension of the cueing volume being 29.7 km) and in the range validation region v_r (with $\sigma^r = 90/\sqrt{12}$ m) are found to be 9.50 and 8.31×10^{-2}, respectively, for gate parameter $g = 5$. The tracks obtained by the maximization procedure are validated using the hypothesis testing as described in Section 3.4. The track acceptance threshold τ_1 was set so that the tracks are accepted with 95% probability (the track acquisition probability $P_{\rm ACQ}$). Figures 6(a) and (b) show the initial points and final points of the accepted tracks formed from the estimates in 100 Monte Carlo runs. The number of validated tracks is 93 (which matches well the acceptance threshold set for 95%) and it can be seen that these accepted tracks fall in the corresponding 95% uncertainty ellipses. In Table 4, the average position and velocity estimates and their corresponding variances are given. The theoretical CRLB of achievable estimator accuracy for the scenario under consideration are given by $\sigma_{\rm CRLB}$. The sample standard deviations of the estimates obtained by the ML/PDA estimator are denoted by $\hat{\sigma}$. For initialization, a systematic grid search is performed to find an approximate maximum point to start off the quasi-Newton maximization procedure. The range of values given to the parameters for this grid search are given by $x_0^{\rm init}$ with 10 points chosen in each component. It can be seen that the sample variance of the estimates is slightly less than the theoretical variance in some cases. This can be explained by the fact that the CRLB models the false alarms as uniformly distributed over the search region while, as can be seen from Fig. 5, they tend to be centered in the beams.

The RMS errors indicate the efficiency of the estimator by considering only the diagonal terms of the covariance matrix as in Table 4. A more rigorous test of the efficiency of the estimator is obtained by checking the consistency of the estimator where the entire error vector and the theoretical covariance are tested for consistency. This is performed by finding the average normalized estimation error squared (NEES) (Bar-Shalom, *et. al.*, 1998) and checking whether it falls within the statistical bounds for acceptance. The NEES is defined as

$$\alpha^{ML} = [\hat{x}_0 - x_0^{\rm true}]' P^{-1} [\hat{x}_0 - x_0^{\rm true}] \quad (94)$$

where $P^{-1} = J$ is the FIM. If the estimator is unbiased and the errors are Gaussian with covariance equal to the CRLB, then α_{ML} defined above is chi-squared distributed with n_x (i.e., 6 in our problem) degrees of freedom. Taking the average over N Monte Carlo runs, the 95% probability bounds on $\bar{\alpha}_{ML}$ are

$$\frac{\chi^2_{6N}(0.975)}{N} \leq \bar{\alpha}_{ML} = \frac{1}{N}\sum_{i=1}^{N} \alpha_i^{ML} \leq \frac{\chi^2_{6N}(0.025)}{N} \quad (95)$$

where α_i^{ML} is the NEES in the i^{ith} Monte Carlo run. If the filter is inefficient or biased then $\bar{\alpha}_{ML}$ will lie outside these bounds. In our simulation the average value of NEES for the accepted tracks is found to be 5.96, which is within the 95% bound (Bar-Shalom, *et. al.*, 1998), namely,

$$\frac{\chi^2_{558}(0.025)}{93} = 5.31 \leq 5.96 \leq \frac{\chi^2_{558}(0.975)}{93} = 6.72 \quad (96)$$

Hence it can be said that the estimator is efficient, i.e., it extracted all the information available in the data.

To evaluate the algorithm's capability of rejecting false tracks (which as discussed earlier, cannot be done theoretically), 1000 runs were carried out with no target present. In these runs, no track was accepted as a valid track. The computation time for one run was 11.18 minutes on a Pentium 200 processor; however, the 10^6 point grid evaluation of the likelihood ratio to initialize the quasi-Newton search took about 11.07 minutes. Since this is easily parallelizable with high efficiency, the effective computation time can be around 10 s for such a (very slow) processor.

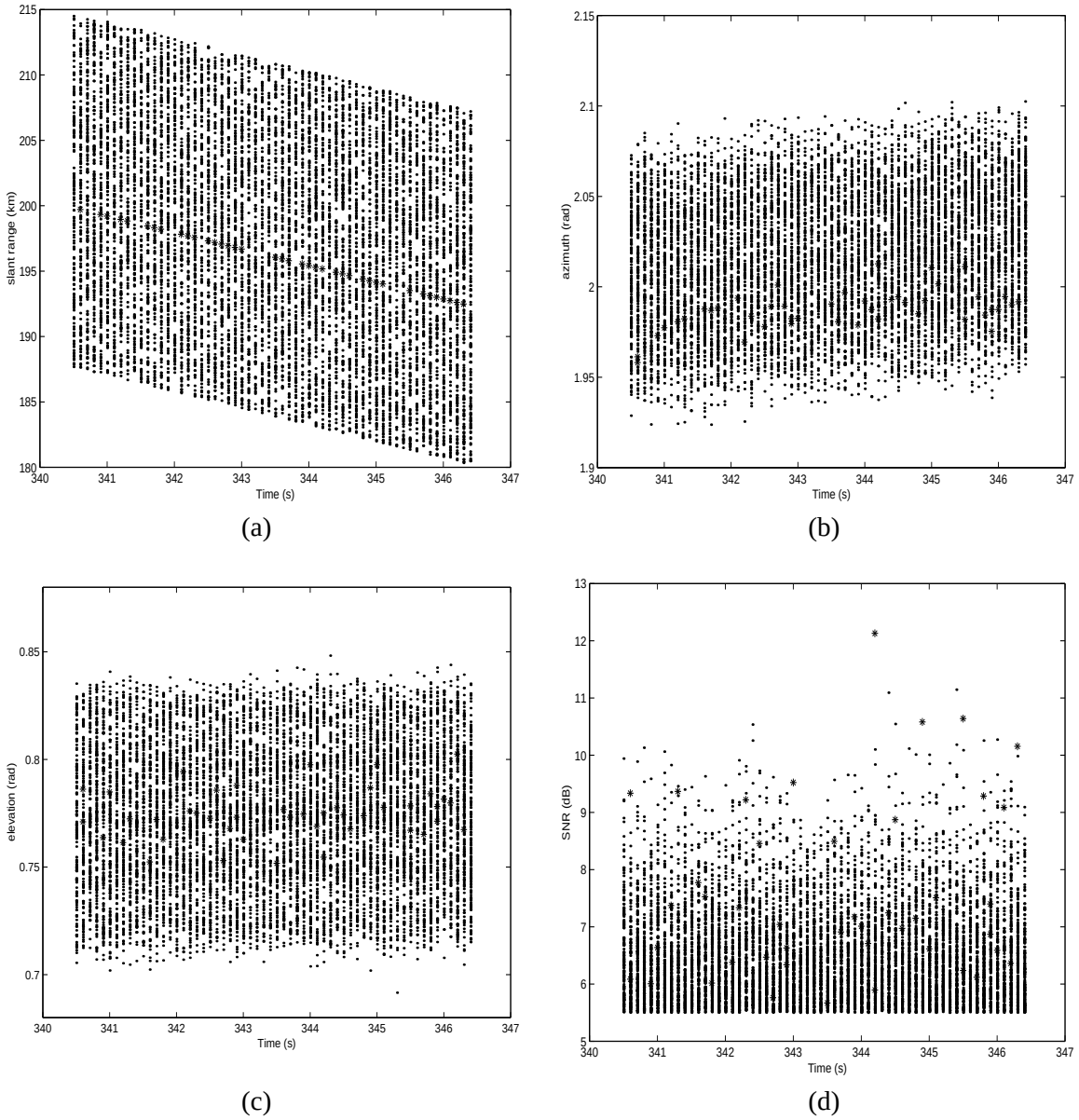

Figure 5: Measurements (one realization): (a) slant range; (b) azimuth; (c) elevation; (d) SNR (* - target originated; · - false alarms).

Parameter	x_0^{true}	Unit	x_0^{init}	$\bar{x}$	σ_{CRLB}	$\hat{\sigma}$
η_0	-56.540	km	$[-70 \quad -40]$	-56.623	0.694	0.703
ξ_0	131.651	km	$[115 \quad 145]$	131.777	0.895	0.637
ζ_0	139.371	km	$[125 \quad 155]$	138.967	0.933	0.816
$\dot{\eta}_0$	6.728	m/s	$[-500 \quad 500]$	28.7	201.6	172.7
$\dot{\xi}_0$	-1557.51	m/s	$[-2000 \quad -1000]$	-1604.5	260.1	191.9
$\dot{\zeta}_0$	-770.982	m/s	$[-1500 \quad -500]$	-622.3	271.7	201.9

Table 2: Results of Monte Carlo simulations.

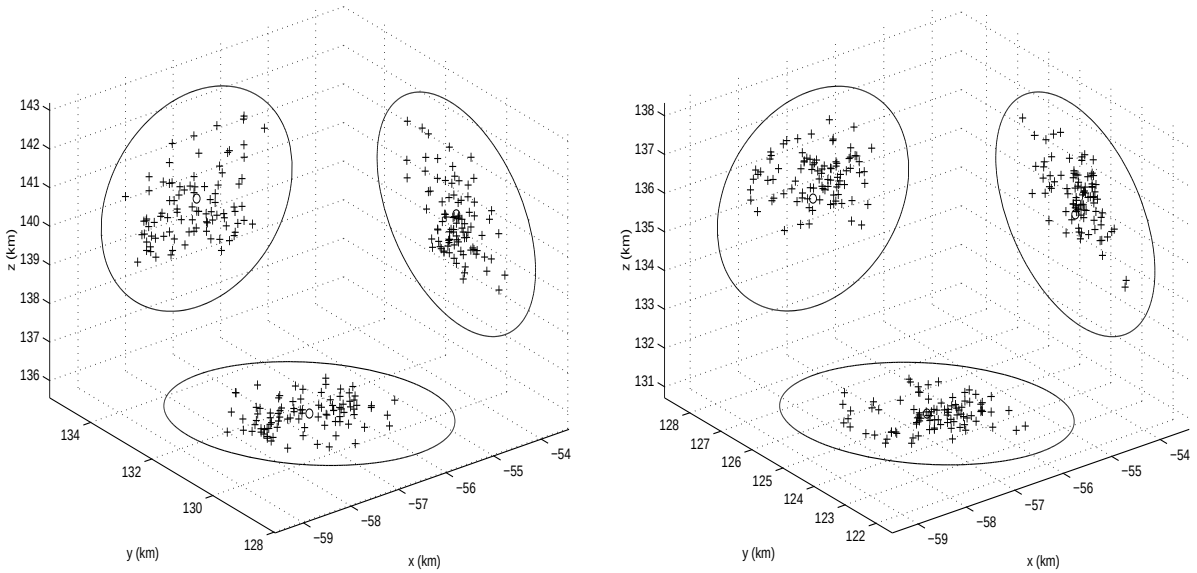

Figure 6: Actual and estimated positions of the missile in 100 Monte Carlo runs with the 95% probability regions from the CRLB (a) initial; (b) final (o - actual + - estimates).

5 Conclusions

The important problem of acquiring an incoming ballistic missile using a surface based ESA radar under low SNR conditions is addressed in this paper. The major technical challenge in this problem is to acquire the missile using the observations available for a short time. It is also necessary to acquire the missile at a long range so that the terminal phase defense systems are able to track the target and take proper action. The problem is compounded by the presence of false alarms due to the low detection threshold made necessary by the target's low radar cross section. An algorithm to estimate the state parameters of a ballistic missile from the observations obtained for a very short duration while the missile is exo-atmospheric is presented. The exact ballistic motion equations are used in this nonlinear acquisition problem. A batch maximum likelihood estimator which can handle false alarms and missed detections using the Probabilistic Data Association approach is derived. It is shown that the incorporation of the amplitude information (signal strength) facilitates the accurate operation of the estimator even under very low SNR conditions. Typically, ESA radars operate at around 13 dB SNR, whereas the new estimator is shown to be effective even at 4 dB, which adds capability for the acquisition of stealthy targets. In other words, this algorithm acts as an effective power multiplier for the radar by a factor of 6. This substantial improvement compared to the existing systems also allows the surface based radar to increase its acquisition range.

In addition to the ML/PDA estimator, a track validation scheme, which is used to confirm the presence of an incoming missile at the estimated location, is also derived. The Cramer-Rao Lower Bound (CRLB), which quantifies the attainable estimator accuracies for this low-observable estimation problem, is also presented. The information reduction factor which accounts for the loss of information due to the presence of false alarms and less-than-unity probability of detection is calculated for different detection thresholds. Hence the optimum detection threshold of the radar can be determined as the threshold that gives the highest value of information reduction factor. Monte Carlo simulations show that the ML/PDA estimator meets the CRLB. The estimator and the CRLB are derived assuming a Swerling III type target, which shows a wide fluctuation in its radar cross section. However, the work can be extended to other

target models as well. The efficiency of the estimator (its ability to extract all the information available in the measurements) under low SNR conditions allows the best utilization of such defense sensors.

APPENDIX A. ALGORITHM FOR BALLISTIC STATE PROPAGATION

An algorithm for propagating the state of a target on a ballistic exo-atmospheric trajectory around the earth is presented in this Appendix. Let the unknown state of the target in the ECI frame at time t_i be denoted by the vector $\mathbf{x}_i^{\text{ECI}} = [\mathbf{r}_i' \;\; \dot{\mathbf{r}}_i']' = \mathbf{f}(\mathbf{x}_0^{\text{ECI}}, t_0, t_i)$. The reference state $\mathbf{x}_0^{\text{ECI}} = [\mathbf{r}_0' \;\; \dot{\mathbf{r}}_0']'$ at the reference time t_0 is given. The underlying theoretical concepts and the derivation of the equations can be found in (Bate, *et. al.*, 1971). The gravitational parameter $\mu = 3.986012 \times 10^5 km^3/s^2$ and the convergence check parameter TOL$= 10^{-10}$.

Step 1

$$r_0 = ||\mathbf{r}_0|| \tag{97}$$

$$\nu_0 = ||\dot{\mathbf{r}}_0|| \tag{98}$$

$$q_0 = \frac{1}{\mu}\mathbf{r}_0'\dot{\mathbf{r}}_0 \tag{99}$$

$$a_0 = \frac{2}{r_0} - \frac{\nu_0^2}{\mu} \tag{100}$$

$$p_0 = \frac{1 - a_0 r_0}{\sqrt{\mu}} \tag{101}$$

Step 2

if$(a_0 \geq 0)$

$$\alpha = a_0(t_i - t_0)\sqrt{\mu} \tag{102}$$

else

$$\alpha = \frac{\text{sign}(t_i - t_0)}{\sqrt{-a_0}} \log\left(\frac{2(\sqrt{-a_0})^3(t_i - t_0)}{q_0\sqrt{-a_0} + p_0 \text{sign}(t_i - t_0)}\right) \tag{103}$$

Step 3

$$\beta = a_0\alpha^2 \tag{104}$$

if$(a_0 \geq 0)$

$$c = \frac{1 - \cos(\sqrt{\beta})}{\beta} \tag{105}$$

$$s = \frac{\sqrt{\beta} - \sin(\sqrt{\beta})}{\beta\sqrt{\beta}} \tag{106}$$

else

$$c = \frac{1 - \cosh(\sqrt{-\beta})}{\beta} \tag{107}$$

$$s = \frac{\sinh(\sqrt{-\beta} - \sqrt{-\beta})}{\beta\sqrt{-\beta}} \tag{108}$$

Step 4

$$\tau = p_0\alpha^3 s + q_0\alpha^2 c + \frac{r_0}{\sqrt{\mu}}\alpha \tag{109}$$

$$\frac{d\tau}{d\alpha} = p_0\alpha^2 c + q_0\alpha(1-s\beta) + \frac{r_0}{\sqrt{\mu}} \quad (110)$$

$$\alpha := \alpha + \left[\frac{d\tau}{d\alpha}\right]^{-1}[(t_i - t_0) - \tau] \quad (111)$$

Step 5

$$\text{if}([(t_i - t_0) - \tau] > \text{TOL})$$

go to Step 3

Step 6

$$h_1 = 1 - \frac{\alpha^2 c}{r_0} \quad (112)$$

$$g_1 = (t_i - t_0) - \frac{\alpha^3 s}{\sqrt{\mu}} \quad (113)$$

$$\mathbf{r}_i = h_1\mathbf{r}_0 + g_1\dot{\mathbf{r}}_0 \quad (114)$$

$$r = ||\mathbf{r}_i|| \quad (115)$$

Step 7

$$h_2 = \left(\frac{\sqrt{\mu}}{r_0}\right)(s\beta - 1)\left(\frac{\alpha}{r}\right) \quad (116)$$

$$g_2 = 1 - \frac{\alpha^2 c}{r} \quad (117)$$

$$\dot{\mathbf{r}}_i = h_2\mathbf{r}_0 + g_2\dot{\mathbf{r}}_0 \quad (118)$$

APPENDIX B. CALCULATION OF PARTIAL DERIVATIVES OF THE STATE

In order to evaluate the FIM, it is necessary to find the 6×3 matrix $\nabla_{\mathbf{x}_0^{\mathrm{R}}}\mathbf{p}_i'$ where $\mathbf{x}_0^{\mathrm{R}} = [\mathbf{p}_0' \;\; \dot{\mathbf{p}}_0']'$ is the state of the target in the radar coordinate frame at the reference time t_0. The state of the target at time t_i, in the ECEF frame is denoted by $\mathbf{x}_i^{\mathrm{ECEF}} = [\mathbf{q}_i' \;\; \dot{\mathbf{q}}_i']'$ and the corresponding state in the ECI frame is denoted by $\mathbf{x}_i^{\mathrm{ECI}} = [\mathbf{r}_i' \;\; \dot{\mathbf{r}}_i']'$. The position vectors $\mathbf{q}_i$ and $\mathbf{r}_i$ are related to each other by

$$\mathbf{q}_i = T_i\,\mathbf{r}_i \quad (119)$$

where T_i is the transformation matrix.

$$T_i = \begin{bmatrix} \cos(\theta_i) & \sin(\theta_i) & 0 \\ -\sin(\theta_i) & \cos(\theta_i) & 0 \\ 0 & 0 & 1 \end{bmatrix} \quad (120)$$

where θ_i is the angle to the prime meridian at the equator, measured in the direction of rotation of the earth, with reference to the vernal equinox direction. The relationship between the position vectors in the radar coordinate frame and the ECEF frame is given by

$$\mathbf{p}_i = \Gamma\,[\mathbf{q}_i - \mathbf{q}_{\mathrm{radar}}] \quad (121)$$

where $\mathbf{q}_{\mathrm{radar}}$ is the radar's position vector in the ECEF frame. The transformation matrix Γ is given by

$$\Gamma = \begin{bmatrix} \cos(\alpha)\cos(\beta+\pi/2) & \sin(\alpha)\cos(\beta+\pi/2) & \sin(\beta+\pi/2) \\ \sin(\alpha) & -\cos(\alpha) & 0 \\ \cos(\alpha)\sin(\beta+\pi/2) & \sin(\alpha)\sin(\beta+\pi/2) & -\cos(\beta+\pi/2) \end{bmatrix} \quad (122)$$

where α and β are the longitude and latitude of the radar, respectively. It can be shown that the gradient of $\mathbf{r}_i$ is given by

$$\nabla_{x_0^{\mathrm{R}}}\mathbf{p}_i' = \nabla_{x_0^{\mathrm{R}}}\mathbf{x}_0'^{\mathrm{ECI}}\nabla_{x_0^{\mathrm{ECI}}}\mathbf{r}_i'\,T_i'\,\Gamma' \tag{123}$$

Similar transformations at reference time t_0 result in

$$\nabla_{x_0^{\mathrm{R}}}\mathbf{x}_0'^{\mathrm{ECI}} = \begin{bmatrix} \Gamma\,T_0 & 0_{3\times 3} \\ 0_{3\times 3} & \Gamma\,T_0 \end{bmatrix} \tag{124}$$

which can be substituted in (123). The 6×3 matrix $\nabla_{x_0^{\mathrm{ECI}}}\mathbf{r}_i'$ can be evaluated with the additional steps given below where the superscript ECI has been dropped.

Step 8

$$\nabla_{\mathbf{x}} r_0 = \begin{bmatrix} \mathbf{r}_0 \\ 0_{3\times 1} \end{bmatrix} \left(\frac{1}{r_0}\right) \tag{125}$$

$$\nabla_{\mathbf{x}} \nu_0 = \begin{bmatrix} 0_{3\times 1} \\ \dot{\mathbf{r}}_0 \end{bmatrix} \left(\frac{1}{\nu_0}\right) \tag{126}$$

$$\nabla_{\mathbf{x}} q_0 = \begin{bmatrix} \dot{\mathbf{r}}_0 \\ \mathbf{r}_0 \end{bmatrix} \left(\frac{1}{\mu}\right) \tag{127}$$

$$\nabla_{\mathbf{x}} a_0 = (\nabla_{\mathbf{x}} r_0)\left(\frac{-2}{r_0^2}\right) + (\nabla_{\mathbf{x}}\nu_0)\left(\frac{-2\nu_0}{\mu}\right) \tag{128}$$

$$\nabla_{\mathbf{x}} p_0 = (\nabla_{\mathbf{x}} r_0)\left(\frac{-a_0}{\sqrt{\mu}}\right) + (\nabla_{r_0} a_0)\left(\frac{-r_0}{\sqrt{\mu}}\right) \tag{129}$$

step 9

$$\frac{dc}{d\beta} = \frac{1 - s\beta - 2c}{2\beta} \tag{130}$$

$$\frac{ds}{d\beta} = \frac{c - 3s}{2\beta} \tag{131}$$

Step 10

$$A = \begin{bmatrix} 3p_0\alpha^2 s + 2q_0\alpha c + \frac{r_0}{\sqrt{\mu}} & p_0\alpha^3\frac{ds}{d\beta} + q_0\alpha^2\frac{dc}{d\beta} \\ 2a_0\alpha & -1 \end{bmatrix} \tag{132}$$

$$b_1 = \nabla_{\mathbf{x}} q_0(-\alpha^2 c) + \nabla_{\mathbf{x}} p_0(-\alpha^3 s) + \nabla_{\mathbf{x}} r_0\left(\frac{-\alpha}{\sqrt{\mu}}\right) \tag{133}$$

$$b_2 = (\nabla_{\mathbf{x}} a_0)(-\alpha^2) \tag{134}$$

$$[\nabla_{\mathbf{x}}\alpha \;\; \nabla_{\mathbf{x}}\beta] = [b_1\, b_2]A^{-1} \tag{135}$$

Step 11

$$\nabla_{\mathbf{x}} h_1 = \left[\nabla_{\mathbf{x}} r_0\frac{\alpha c}{r_0} - (\nabla_{\mathbf{x}}\alpha)(2c) - (\nabla_{\mathbf{x}}\beta)\left(\alpha\frac{dc}{d\beta}\right)\right]\left[\frac{\alpha}{r_0}\right] \tag{136}$$

$$\nabla_{\mathbf{x}} g_1 = \left[(\nabla_{\mathbf{x}}\alpha)(3s) - (\nabla_{\mathbf{x}}\beta)\left(\alpha\frac{ds}{d\beta}\right)\right]\left[\frac{-\alpha^2}{\sqrt{\mu}}\right] \tag{137}$$

Step 12

$$\nabla_{\mathbf{x}}\mathbf{r}_i' = \begin{bmatrix} h_1 I_3 \\ g_1 I_3 \end{bmatrix} + (\nabla_{\mathbf{x}} h_1)(\mathbf{r}_0') + (\nabla_{\mathbf{x}} g_1)(\dot{\mathbf{r}}_0') \tag{138}$$

APPENDIX C. DERIVATION OF FISHER INFORMATION MATRIX (FIM)

The steps followed in the derivation of the FIM are based on (Kirubarajan, *et. al.*, 1996). The FIM can be written as the sum of the individual FIMs J_i at t_i. That is

$$J = \sum_{i=1}^{N} J_i \tag{139}$$

J_i is defined as

$$J_i = E\{\nabla_{\mathbf{x}} \ln p[Z(i)|\mathbf{x}] \nabla'_{\mathbf{x}} \ln p[Z(i)|\mathbf{x}]\}|_{\mathbf{x}=\mathbf{x}^{\text{true}}} \tag{140}$$

where $p[Z(i)|\mathbf{x}]$ is defined as in (57) and $\mathbf{x}$ is the state of the missile at the reference time.

It is assumed that the false alarms are distributed uniformly in the validation region of volume v_g given in (73). Also the Swerling RCS parameter α_{ik}, normalized radiation pattern Σ_{ik}, and the angle measurement standard deviations σ_{ik}^{β}, σ_{ik}^{ϵ} are substituted with their average values. Then from (57), one has

$$\begin{aligned} p[Z(i)|\mathbf{x}] &= \mu_g(m_i) \prod_{j=1}^{m_i} p_0^{\tau}(\Re_{ij}) p_0(r_{ij}) p_0(\beta_{ij}) p_0(\epsilon_{ij}) \\ &\quad \left\{ \frac{\mu_g(m_i - 1) P_D \, v_g}{m_i \mu_g(m_i) (\sqrt{2\pi})^3 \sigma^r \sigma^{\beta} \sigma^{\epsilon}} \sum_{k=1}^{m_i} \rho_{ik} \, \exp(\varphi(z_{ik}, \mathbf{x})) + (1 - P_D) \right\} \end{aligned} \tag{141}$$

where

$$\varphi(z_{ik}, \mathbf{x}) = -\frac{(r_{ik} - r_i(\mathbf{x}))^2}{2(\sigma^r)^2} - \frac{(\beta_{ik} - \beta_i(\mathbf{x}))^2}{2(\sigma^{\beta})^2} - \frac{(\epsilon_{ik} - \epsilon_i(\mathbf{x}))^2}{2(\sigma^{\epsilon})^2} \tag{142}$$

Using (35) one has

$$p[Z(i)|\mathbf{x}] = \exp\left\{ \sum_{k=1}^{m_i} \Re_{ik} \right\} \left\{ a \sum_{k=1}^{m_i} \rho_{ik} \exp\{\varphi(z_{ik}, \mathbf{x})\} + b \right\} \tag{143}$$

where

$$a = \frac{P_D \mu_g(m_i - 1) v_g^{1-m_i} P_{FA}^{-m_i}}{m_i (\sqrt{2\pi})^3 \sigma^r \sigma^{\beta} \sigma^{\epsilon}} \tag{144}$$

$$b = (1 - P_D) \mu_g(m_i) (v_g P_{FA})^{-m_i} \tag{145}$$

$$\mu_g(m_i) = \frac{e^{-\lambda_g v_g} (\lambda_g v_g)^{m_i}}{m_i!} \tag{146}$$

where λ_g is the expected number of false alarms per unit volume. From (52)

$$\rho_{ik} = \theta(1 + \nu \Re_{ik}) \exp\{\nu \Re_{ik}\} \tag{147}$$

where θ and ν come from (54) and (55), respectively, with the average values of α_{ik} and Σ_{ik}. Then $\nabla_{\mathbf{x}} \ln p[Z(i)|\mathbf{x}]$ can be shown to be

$$\nabla_{\mathbf{x}} \ln p[Z(i)|\mathbf{x}] = \frac{a \sum_{k=1}^{m_i} \rho_{ik} \exp\{\varphi(z_{ik}, \mathbf{x})\} [\nabla_{\mathbf{x}} \varphi(z_{ik}, \mathbf{x})]}{a \sum_{k=1}^{m_i} \rho_{ik} \exp\{\varphi(z_{ik}, \mathbf{x})\} + b} \tag{148}$$

Substituting (148) in (140) and observing that the cross terms vanish due to the independence of measurements across the scans, one has

$$\begin{aligned} J_i &= \sum_{m_i=1}^{\infty} a(\sigma^r\sigma^\beta\sigma^\epsilon)^{m_i} \int_\tau^\infty \cdots \int_\tau^\infty \int_{R_1}^{R_2} \cdots \int_{R_1}^{R_2} \int_{\beta_1}^{\beta_2} \cdots \int_{\beta_1}^{\beta_2} \int_{\epsilon_1}^{\epsilon_2} \cdots \int_{\epsilon_1}^{\epsilon_2} \\ &\quad \times \frac{a^2 \exp\{-\sum_{j=1}^{m_i} \Re_{ij}\} \sum_{k=1}^{m_i} \rho_{ik}^2 \exp\{2\varphi(z_{ik},\mathbf{x})\} [\nabla_{\mathbf{x}}\varphi(z_{ik},\mathbf{x})][\nabla_{\mathbf{x}}\varphi(z_{ik},\mathbf{x})]'}{a\sum_{k=1}^{m_i} \rho_{ik} \exp\{\varphi(z_{ik},\mathbf{x})\} + b} \, dZ(i) \end{aligned} \tag{149}$$

Letting

$$\xi = \begin{bmatrix} \xi_{11} \\ \xi_{12} \\ \xi_{13} \\ \vdots \\ \xi_{m_i 1} \\ \xi_{m_i 2} \\ \xi_{m_i 3} \end{bmatrix} = \begin{bmatrix} (r_{i1} - r_i(\mathbf{x}))/\sigma^r \\ (\beta_{i1} - \beta_i(\mathbf{x}))/\sigma^\beta \\ (\epsilon_{i1} - \epsilon_i(\mathbf{x}))/\sigma^\epsilon \\ \vdots \\ (r_{im_i} - r_i(\mathbf{x}))/\sigma^r \\ (\beta_{im_i} - \beta_i(\mathbf{x}))/\sigma^\beta \\ (\epsilon_{im_i} - \epsilon_i(\mathbf{x}))/\sigma^\epsilon \end{bmatrix} \tag{150}$$

results in the expression

$$\begin{aligned} J_i &= \sum_{m_i=1}^{\infty} a(\sigma^r\sigma^\beta\sigma^\epsilon)^{m_i} \int_\tau^\infty \cdots \int_\tau^\infty \int_{-g}^{g} \cdots \int_{-g}^{g} \int_{-g}^{g} \cdots \int_{-g}^{g} \int_{-g}^{g} \cdots \int_{-g}^{g} \\ &\quad \times \frac{\exp\{-\sum_{j=1}^{m_i} \Re_{ij}\} \sum_{k=1}^{m_i} \rho_{ik}^2 \exp\{-(\xi_{k1}^2 + \xi_{k2}^2 + \xi_{k3}^2)\} [\Delta_{ik}][\Delta_{ik}]'}{\sum_{k=1}^{m_i} \rho_{ik} \exp\{-\frac{1}{2}(\xi_{k1}^2 + \xi_{k2}^2 + \xi_{k3}^2)\} + b/a} \, d\xi \, d\Re \end{aligned} \tag{151}$$

where

$$\begin{aligned} [\Delta_{ik}][\Delta_{ik}]' &= \left\{ \frac{\xi_{k1}^2}{(\sigma^r)^2} [\nabla_{\mathbf{x}} r_i(\mathbf{x})][\nabla_{\mathbf{x}} r_i(\mathbf{x})]' + \frac{\xi_{k2}^2}{(\sigma^\beta)^2} [\nabla_{\mathbf{x}} \beta_i(\mathbf{x})][\nabla_{\mathbf{x}} \beta_i(\mathbf{x})]' \right. \\ &\quad \left. \frac{\xi_{k3}^2}{(\sigma^\epsilon)^2} [\nabla_{\mathbf{x}} \epsilon_i(\mathbf{x})][\nabla_{\mathbf{x}} \epsilon_i(\mathbf{x})]' \right\} \end{aligned} \tag{152}$$

Because of the symmetry of the integration, J_i can be simplified to

$$\begin{aligned} J_i &= \sum_{m_i=1}^{\infty} a(\sigma^r\sigma^\beta\sigma^\epsilon)^{m_i} m_i \int_\tau^\infty \cdots \int_\tau^\infty \int_{-g}^{g} \cdots \int_{-g}^{g} \int_{-g}^{g} \cdots \int_{-g}^{g} \int_{-g}^{g} \cdots \int_{-g}^{g} \\ &\quad \times \frac{\exp\{-\sum_{j=1}^{m_i} \Re_{ij}\} \rho_{i1}^2 \exp\{-(\xi_{11}^2 + \xi_{12}^2 + \xi_{13}^2)\} \xi_{11}^2}{\sum_{k=1}^{m_i} \rho_{ik} \exp\{-\frac{1}{2}(\xi_{k1}^2 + \xi_{k2}^2 + \xi_{k3}^2)\} + b/a} \, d\xi \, d\Re \, J_{0i} \end{aligned} \tag{153}$$

where

$$J_{0i} = \frac{1}{(\sigma^r)^2} [\nabla_{\mathbf{x}} r_i(\mathbf{x})][\nabla_{\mathbf{x}} r_i(\mathbf{x})]' + \frac{1}{(\sigma^\beta)^2} [\nabla_{\mathbf{x}} \beta_i(\mathbf{x})][\nabla_{\mathbf{x}} \beta_i(\mathbf{x})]' + \frac{1}{(\sigma^\epsilon)^2} [\nabla_{\mathbf{x}} \epsilon_i(\mathbf{x})][\nabla_{\mathbf{x}} \epsilon_i(\mathbf{x})]' \tag{154}$$

Defining

$$\begin{aligned} I_1 &= \int_\tau^\infty \cdots \int_\tau^\infty \int_0^g \cdots \int_0^g \int_0^g \cdots \int_0^g \int_0^g \cdots \int_0^g \\ &\quad \times \frac{\exp\{-\sum_{j=1}^{m_i} \Re_{ij}\} \rho_{i1}^2 \exp\{-(\xi_{11}^2 + \xi_{12}^2 + \xi_{13}^2)\} \xi_{11}^2}{\sum_{k=1}^{m_i} \rho_{ik} \exp\{-\frac{1}{2}(\xi_{k1}^2 + \xi_{k2}^2 + \xi_{k3}^2)\} + b/a} \, d\xi \, d\Re \end{aligned} \tag{155}$$

J_i can be written as

$$J_i \;=\; \sum_{m_i=1}^{\infty} a(\sigma^r\sigma^\beta\sigma^\epsilon)^{m_i} m_i 2^{3m_i} I_1 J_{0i} \tag{156}$$

Substituting for ρ_{i1} in (155) from (147)

$$\begin{aligned} I_1 \;=\; & \int_\tau^\infty \cdots \int_\tau^\infty \int_0^g \cdots \int_0^g \int_0^g \cdots \int_0^g \int_0^g \cdots \int_0^g \\ & \times \frac{\exp\{-\sum_{j=1}^{m_i} \Re_{ij}\}\theta^2(1+\nu\Re_{i1})^2 \exp\{2\nu\Re_{i1} - (\xi_{11}^2+\xi_{12}^2+\xi_{13}^2)\}\xi_{11}^2}{\sum_{k=1}^{m_i}\theta(1+\nu\Re_{ik})\exp\{\nu\Re_{ik} - \frac{1}{2}(\xi_{k1}^2+\xi_{k2}^2+\xi_{k3}^2)\} + b/a}\, d\xi\, d\Re \end{aligned} \tag{157}$$

Finally, substituting a and b with their values defined in (144) and (145) and denoting

$$\begin{aligned} I_2(m_i, P_D, \lambda_g v_g, \alpha\Sigma^4) \;=\; & \int_\tau^\infty \cdots \int_\tau^\infty \int_0^g \cdots \int_0^g \int_0^g \cdots \int_0^g \int_0^g \cdots \int_0^g \\ & \times \frac{\exp\{-\sum_{j=1}^{m_i} \Re_{ij}\}(1+\nu\Re_{i1})^2 \exp\{2\nu\Re_{i1} - (\xi_{11}^2+\xi_{12}^2+\xi_{13}^2)\}\xi_{11}^2}{\sum_{k=1}^{m_i}(1+\nu\Re_{ik})\exp\{\nu\Re_{ik} - \frac{1}{2}(\xi_{k1}^2+\xi_{k2}^2+\xi_{k3}^2)\} + \left(\frac{\sqrt{2\pi}}{2g}\right)^3 \frac{(1-P_D)\lambda_g v_g}{P_D\theta}}\, d\xi\, d\Re \end{aligned} \tag{158}$$

one has

$$J_i \;=\; \sum_{m_i=1}^{\infty} \frac{2^6\,\mu_g(m_i-1)P_{FA}^{1-m_i}}{\pi\sqrt{2\pi}\,g^{3m_i-3}(4+\alpha\Sigma^4)^2} I_2(m_i, P_D, \lambda_g v_g, \alpha\Sigma^4) J_{0i} \tag{159}$$

Defining

$$q(P_D, \lambda_g v_g, g, \alpha\Sigma^4) \;=\; \sum_{m_i=1}^{\infty} \frac{2^6\,\mu(m_i-1)P_{FA}^{1-m_i}}{\pi\sqrt{2\pi}\,g^{3m_i-3}(4+\alpha\Sigma^4)^2} I_2(m_i, P_D, \lambda_g v_g, \alpha\Sigma^4) \tag{160}$$

the FIM can be written as

$$J \;=\; q(P_D, \lambda_g v_g, g, \alpha\Sigma^4) \sum_{i=1}^{N} J_{0i} \tag{161}$$

The numerical values of $q(P_D, \lambda_g v_g, g, \alpha\Sigma^4)$ for different probabilities of detection with the fixed 4dB effective average SNR are presented in Table 3. As it can be seen from this table, $q(\cdot)$ does not vary significantly with the threshold τ. Tables 4, 5, 6, 7 and 8 present the numerical values of $q(\cdot)$ for the fixed effective average SNR of 8dB, 10dB, 12dB, 14dB and 16dB.

τ	3.80	3.31	3.22	3.14	2.62	2.22
P_D	0.4	0.5	0.6	0.7	0.8	0.9
P_{FA}	0.0224	0.0366	0.0400	0.0431	0.0726	0.1080
$\lambda_g v_g$	0.2973	0.4852	0.5302	0.5722	0.9627	1.4312
$q(\cdot)$	0.4017	0.4225	0.4287	**0.4362**	0.4134	0.3561

Table 3: Values of $q(P_D, \lambda_g v_g, g, \alpha\Sigma^4)$ for $g = 5$ and $\alpha\Sigma^4 = 7.0$ (SNNR = 5.4dB)

τ	5.42	4.57	3.74	3.22	3.01	2.28
P_D	0.4	0.5	0.6	0.7	0.8	0.9
P_{FA}	0.0044	0.0103	0.0238	0.0400	0.04929	0.1022
$\lambda_g v_g$	0.0586	0.1373	0.3155	0.5300	0.6533	1.3558
$q(\cdot)$	0.5131	0.5700	0.6084	**0.6085**	0.6000	0.4628

Table 4: Values of $q(P_D, \lambda_g v_g, g, \alpha\Sigma^4)$ for $g = 5$ and $\alpha\Sigma^4 = 12.6$ (SNR = 8dB)

τ	7.78	6.38	5.28	4.11	3.22	2.31
P_D	0.4	0.5	0.6	0.7	0.8	0.9
P_{FA}	0.0004	0.0017	0.0051	0.0164	0.0400	0.0989
$\lambda_g v_g$	0.0055	0.0223	0.0674	0.2175	0.5302	1.3111
$q(\cdot)$	0.5272	0.6057	0.6654	**0.7153**	0.6984	0.5131

Table 5: Values of $q(P_D, \lambda_g v_g, g, \alpha\Sigma^4)$ for $g = 5$ and $\alpha\Sigma^4 = 20.0$ (SNR = 10dB)

APPENDIX D. DERIVATION OF MOMENTS OF LOG-LIKELIHOOD RATIO UNDER TARGET HYPOTHESIS (H_1)

In deriving the moments of the likelihood ratio, only the measurements which fall into the validation gate are considered. The n-th moment of the log-likelihood ratio at time t_i is

$$E\{(\phi[(i), \mathbf{x}])^n | H_1\} = \sum_{m_i=0}^{\infty} \int_{\tau}^{\infty} \cdots \int_{\tau}^{\infty} \int_{R_1}^{R_2} \cdots \int_{R_1}^{R_2} \int_{\beta_1}^{\beta_2} \cdots \int_{\beta_1}^{\beta_2} \int_{\epsilon_1}^{\epsilon_2} \cdots \int_{\epsilon_1}^{\epsilon_2} \phi[Z(i), \mathbf{x}])^n p[Z(i)|\mathbf{x}]\, dZ(i) \tag{162}$$

where $p[Z(i)|\mathbf{x}]$ is the pdf in (143) of the validated measurements under hypothesis H_1. Using the approximations discussed in Appendix C, the log-likelihood ratio can be written as

$$\phi[Z(i), \mathbf{x}] = \ln \left[\frac{4g^3 P_D}{\pi\sqrt{2\pi}\lambda_g v_g} \sum_{k=1}^{m_i} \rho_{ik} \exp\{\varphi(z_{ik}, \mathbf{x})\} + (1 - P_D) \right] \tag{163}$$

Using the same changes of variables as those introduced in Appendix C, one has

$$E\{(\phi[(i), \mathbf{x}])^n | H_1\} = (1 - P_D)[\ln(1 - P_D)]^n e^{-\lambda_g v_g} \frac{2^6 e^{-\lambda_g v_g}}{\pi\sqrt{2\pi}(4 + \alpha\Sigma^4)^2} \sum_{m_i=1}^{\infty} \frac{P_{FA}^{1-m_i} (\lambda_g v_g)^{m_i - 1}}{m! g^{3m_i - 3}}$$

τ	12.06	9.96	8.11	6.38	4.62	2.35
P_D	0.4	0.5	0.6	0.7	0.8	0.9
P_{FA}	6×10^{-6}	47×10^{-6}	299×10^{-6}	0.0017	0.0098	0.0954
$\lambda_g v_g$	77×10^{-6}	626×10^{-6}	0.0040	0.0224	0.1302	1.2641
$q(\cdot)$	0.4307	0.5136	0.5885	0.6561	**0.7143**	0.4993

Table 6: Values of $q(P_D, \lambda_g v_g, g, \alpha\Sigma^4)$ for $g = 5$ and $\alpha\Sigma^4 = 31.7$ (SNR = 12dB)

τ	18.25	15.07	12.25	9.53	6.56	2.40
P_D	0.4	0.5	0.6	0.7	0.8	0.9
P_{FA}	0	0	5×10^{-6}	73×10^{-6}	0.0014	0.0907
$\lambda_g v_g$	0	4×10^{-6}	63×10^{-6}	0.0010	0.0187	1.2025
$q(\cdot)$	0.2509	0.3344	0.4108	0.4832	**0.5565**	0.4111

Table 7: Values of $q(P_D, \lambda_g v_g, g, \alpha\Sigma^4)$ for $g = 5$ and $\alpha\Sigma^4 = 50.2$ (SNR = 14dB)

τ	28.09	23.21	18.89	14.71	10.04	2.42
P_D	0.4	0.5	0.6	0.7	0.8	0.9
P_{FA}	0	0	0	0	44×10^{-6}	0.0889
$\lambda_g v_g$	0	0	0	5×10^{-6}	0.0006	1.1787
$q(\cdot)$	0.0315	0.1141	0.1901	0.2627	**0.3381**	0.2763

Table 8: Values of $q(P_D, \lambda_g v_g, g, \alpha\Sigma^4)$ for $g = 5$ and $\alpha\Sigma^4 = 79.6$ (SNR = 16dB)

$$\int_\tau^\infty \cdots \int_\tau^\infty \int_0^g \cdots \int_0^g \int_0^g \cdots \int_0^g \int_0^g \cdots \int_0^g$$
$$\times \left\{ \ln \left[\frac{2^6 g^3 P_{FA}}{\pi\sqrt{2\pi}\lambda_g v_g (4+\alpha\Sigma^4)^2} \sum_{k=1}^{m_i} (1+\nu\Re_{ik}) \exp\{\nu\Re_{ik} - \frac{1}{2}(\xi_{k1}^2 + \xi_{k2}^2 + \xi_{k3}^2)\} + (1-P_D) \right] \right\}^n$$
$$\times \left\{ \sum_{k=1}^{m_i} (1+\nu\Re_{ik}) \exp\{\nu\Re_{ik} - \frac{1}{2}(\xi_{k1}^2 + \xi_{k2}^2 + \xi_{k3}^2)\} + \left(\frac{\sqrt{2\pi}}{2g}\right)^3 \frac{(1-P_D)\lambda_g v_g}{P_D \theta} \right\}$$
$$\times \exp\left[-\sum_{j=1}^{m_i} \Re_{ij} \right] \, d\Re \, d\xi \tag{164}$$

The numerical values of the first two moments at SNR= 4dB for different probabilities of detection are presented in Table 9.

τ	3.80	3.31	3.22	3.14	2.62	2.22
P_D	0.4	0.5	0.6	0.7	0.8	0.9
P_{FA}	0.0224	0.0366	0.0400	0.0431	0.0726	0.1080
$\lambda_g v_g$	0.2973	0.4852	0.5302	0.5722	0.9627	1.4312
μ_1	1.7886	1.7429	1.7024	1.6760	1.4734	1.1958
σ_1	3.0813	3.0442	3.0580	3.0534	2.8776	2.6012

Table 9: Values of μ_1 and σ_1 for $g = 5$ and $\alpha\Sigma^4 = 7.0$ (SNR = 4dB)

APPENDIX E. DERIVATION OF MOMENTS OF LOG-LIKELIHOOD RATIO UNDER NO TARGET HYPOTHESIS (H_0)

When there is no target, the n-th moment of the log-likelihood ratio of the measurements in the validation region at time t_i is

$$\begin{aligned}\{(\phi[(i),\mathbf{x}])^n|H_0\} &= \sum_{m_i=0}^{\infty}\int_{\tau}^{\infty}\cdots\int_{\tau}^{\infty}\int_{R_1}^{R_2}\cdots\int_{R_1}^{R_2}\int_{\beta_1}^{\beta_2}\cdots\int_{\beta_1}^{\beta_2}\int_{\epsilon_1}^{\epsilon_2}\cdots\int_{\epsilon_1}^{\epsilon_2} \\ &\quad (\phi[Z(i),\mathbf{x}])^n p[Z(i)|H_0]\,dZ(i)\end{aligned} \tag{165}$$

where $\phi[Z(i),\mathbf{x}]$ is the same as in (163) and $p[Z(i)|H_0]$ is given by

$$p[Z(i)|H_0] = \frac{\lambda_g^{m_i} e^{-\lambda_g v_g} P_{FA}^{-m_i}}{m_i!}\exp\left\{-\sum_{j=1}^{m_i}\Re_{ij}\right\} \tag{166}$$

After similar manipulations as in Appendix D

$$\begin{aligned}E\{(\phi[(i),\mathbf{x}])^n|H_0\} &= [\ln(1-P_D)]^n e^{-\lambda_g v_g} + \sum_{m_i=1}^{\infty}\frac{e^{-\lambda_g v_g}}{m!}\left(\frac{\lambda_g v_g}{P_{FA} g^3}\right)^{m_i} \\ &\int_{\tau}^{\infty}\cdots\int_{\tau}^{\infty}\int_0^g\cdots\int_0^g\int_0^g\cdots\int_0^g\int_0^g\cdots\int_0^g \\ &\times\left\{\ln\left[\frac{2^6 g^3 P_{FA}}{\pi\sqrt{2\pi}\lambda_g v_g(4+\alpha\Sigma^4)^2}\sum_{k=1}^{m_i}(1+\nu\Re_{ik})\exp\{\nu\Re_{ik}-\frac{1}{2}(\xi_{k1}^2+\xi_{k2}^2+\xi_{k3}^2)\}+(1-P_D)\right]\right\}^n \\ &\times\exp\left[-\sum_{j=1}^{m_i}\Re_{ij}\right]\,d\Re\,d\xi\end{aligned} \tag{167}$$

The numerical values of the first two moments for different probabilities of detection at SNR $= 4$dB, are presented in Table 10.

τ	3.80	3.31	3.22	3.14	2.62	2.22
P_D	0.4	0.5	0.6	0.7	0.8	0.9
P_{FA}	0.0224	0.0366	0.0400	0.0431	0.0726	0.1080
$\lambda_g v_g$	0.2973	0.4852	0.5302	0.5722	0.9627	1.4312
μ_0	-0.4650	-0.6135	-0.8308	-1.1373	-1.4751	-1.8962
σ_0	0.4166	0.4421	0.5172	0.6384	0.7311	1.1087

Table 10: Values of μ_0 and σ_0 for $g = 5$ and $\alpha\Sigma^4 = 7.0$ (SNR = 4dB)

APPENDIX F. CALCULATION OF PROBABILITY OF DETECTION IN A HEXAGONAL AREA

The probability of detection in a hexagonal region corresponding to the triangular lattice search pattern (square in the rectangular case of Fig. 3(a)) is found by selecting a number of points in this region and

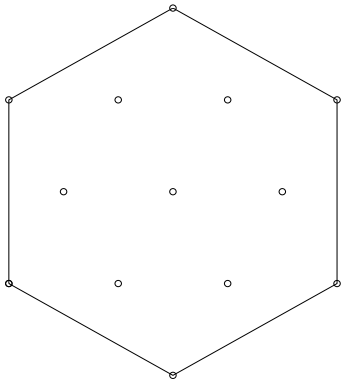

Figure 7: Discretized points in a hexagon where $P_{d_{ijk}}$'s are found.

finding the average of the detection probabilities of those points. The probability of the k-th point at the j-th range bin of the i-th hexagon is taken as

$$P_{d_{ijk}} = 1 - \prod_{m=1}^{n} (1 - P_{d_m}) \tag{168}$$

where P_{d_m} is the probability of detection of a target at the k-th point due to the m-th dwell of the total n dwells. Assuming uniform distribution for the target location over the hexagonal region $P_{d_{ij}}$ used in (2) is calculated using

$$P_{d_{ij}} = \frac{1}{p} \sum_{k=1}^{p} w_k P_{d_{ijk}} \tag{169}$$

where p is the number of points in the hexagon and w_k are the weights given to each of these points depending on their location in the hexagon. At the corners of the hexagon the weights are $1/3$ (because such a point appears in 3 hexagons) and at the ones inside the hexagon the weights are 1.

References

Bar-Shalom, Y., Li, X.R. (1998). *Estimation and Tracking: Principles, Techniques and Software,* Artech House, Norwood, MA. 1993. Reprinted by YBS Publishing, Storrs, CT.

Bar-Shalom, Y., Li, X.R. (1995). *Multitarget - Multisensor Tracking: Principles and Techniques,* YBS Publishing, Storrs, CT.

Barton, D.K.(1964). *Radar System Analysis* Prentice-Hall Inc., Englewood Cliffs, NJ.

Bate, R.R., Mueller, D.D., White, J.E. (1971). *Fundamentals of Astrodynamics,* Dover Publications, NY.

Blair, W.D., Watson, G.A., Kirubarajan, T., Bar-Shalom Y. (1998). "Benchmark for Radar Resource Allocation and Tracking Targets in the Presence of ECM," *IEEE Transactions on Aerospace and Electronic Systems,* **AES 34, 4**.

Bossé, E., Turner, R., Lecours M. (1991). “Tracking Swerling Fluctuating Targets at Low Altitude Over the Sea,” *IEEE Transactions on Aerospace and Electronic Systems*, **AES 27, 5**, 806-821.

Conte, E., Longo, M., Lops, M. (1991). “Modeling and Simulation of Non-Rayleigh Radar Clutter,” *IEE Proceedings-F Radar and Signal Processing*, **IEE-F 138, 2**, 121-131.

Conte, E., Ricci, G. (1994). “Performance Prediction in Compound Gaussian Clutter,” *IEEE Transactions on Aerospace and Electronic Systems*, **AES 30, 2**, 611-616.

Duncan, P. H. (1996). “Overlapping Search With Scanned Beam Applications,” *IEEE Transactions on Aerospace and Electronic Systems*, **AES 32, 3**, 984-994.

Fielding, J. E. (1993). “Beam Overlap Impact on Phased-Array Target Detection,” *IEEE Transactions on Aerospace and Electronic Systems*, **AES 29, 2**, 404-411.

Jauffret, C., Bar-Shalom, Y. (1990). “Track formation with bearing and frequency measurements in clutter,” *IEEE Transactions on Aerospace and Electronic Systems*, **AES 26, 6**, 999-1009.

Kirubarajan, T., Bar-Shalom Y. (1996). “Low Observable Target Motion Analysis Using Amplitude Information,” *IEEE Transactions on Aerospace and Electronic Systems*, **AES 32, 4**, 1367-1384.

Lerro, D., Bar-Shalom, Y. (1993). “Interacting multiple model tracking with target amplitude feature,” *IEEE Transactions on Aerospace and Electronic Systems*, **AES 29, 2**, 494-509.

Li, Y., Yeddanapudi, M., Kirubarajan, T., Bar-Shalom, Y. (1997). “Trajectory and Launch Point Estimation For Ballistic Missiles From Boost Phase LOS Measurements,” *Proceedings of SPIE*, 3163-29.

Mehra, R. K. (1971). “A Comparison of Several Nonlinear Filters for Reentry Vehicle Tracking,” *IEEE Transactions on Automatic Control*, **AC 16, 4**, 307-319.

Poor, H.V. (1994). *An Introduction to Signal Detection and Estimation*, Springer-Verlag, NY.

Press, W.H., Teukolsky, S.A., Vetterling, W.T., Flannery, B.P. (1992). *Numerical Recipes in C*, Cambridge University Press, Cambridge, UK.

Siouris, G.M., Chen, G., Wang, J. (1997). “Tracking an Incoming Ballistic Missile Using an Extended Interval Kalman Filter,” *IEEE Transactions on Aerospace and Electronic Systems*, **AES 33, 1**, 232 - 240.

Skolnik, M. I. (1980). *Introduction to Radar Systems*, McGraw-Hill Book Company, New York.

Swerling, P., Peterman, W.L. (1990). “Impact of Target RCS Fluctuations on Radar Measurement Accuracy,” *IEEE Transactions on Aerospace and Electronic Systems*, **AES 26, 4**, 685-686.

Watson, G. N. (1944). *A Treatise On the Theory of Bessel Functions*, The MacMillan Company, NY.

Yeddanapudi, M., Bar-Shalom, Y., Pattipati, K.R., Deb S. (1997). “Ballistic Missile Track Initiation From Satellite Observations,” *IEEE Transactions on Aerospace and Electronic Systems*, **AES 31, 3**, 1054 - 1071.